NATIONAL ENERGY TECHNOLOGY LABORATORY

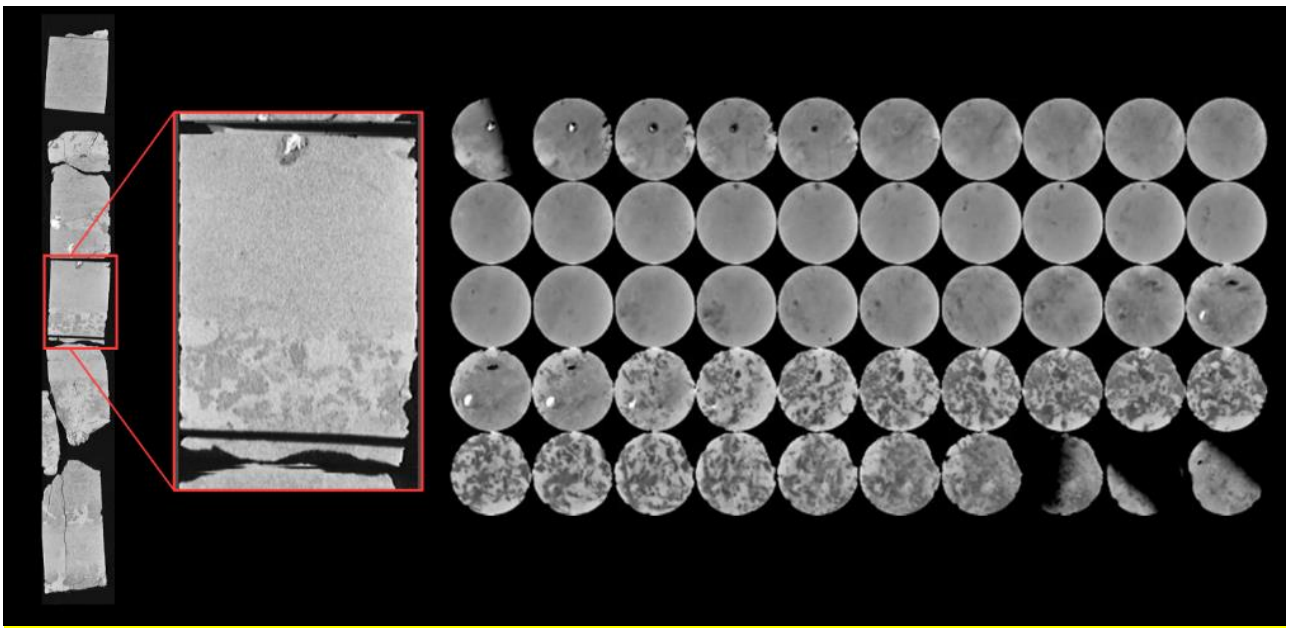

Computed Tomography Scanning and Petrophysical Measurements of the Wellington KGS 2-32 Core

21 January 2022

U.S. DEPARTMENT OF ENERGY | NATIONAL ENERGY TECHNOLOGY LABORATORY

Office of Fossil Energy

DOE/NETL-2022/3725

Disclaimer

Cover Illustration: Medical computed tomography image through the center of core from the Wellington KGS 2-32 well, obtained from a depth of 3,711.9–3,714.7 ft (left), and a montage of cross-sections from this core from a depth of 3,713–3,713.5 ft (right).

Suggested Citation: Schmitt, R.; Paronish, T.; Crandall, D.; Moore, J.; Hasiuk, F.; Potter, N.; Holubnyak, Y. E. *Computed Tomography Scanning and Petrophysical Measurements of the Wellington KGS 2-32 Core;* DOE/NETL-2022/3725; NETL Technical Report Series; U.S. Department of Energy, National Energy Technology Laboratory: Morgantown, WV, 2022; p 60. DOI: 10.2172/1841374

An electronic version of this report can be found at:

https://edx.netl.doe.gov/group/core-characterization and https://netl.doe.gov/energy-analysis

The data in this report can be accessed from NETL's Energy Data eXchange (EDX) online system (https://edx.netl.doe.gov) using the following link: https://edx.netl.doe.gov/dataset/wellington2-32-core

Computed Tomography Scanning and Petrophysical Measurements of the Wellington KGS 2-32 Core

Rhiannon Schmitt[1,2], Thomas Paronish[1,3], Dustin Crandall[1], Johnathan Moore[1,3], Franciszek "Franek" Hasiuk[4], Nicole Potter[4], Yevhen "Eugene" Holubnyak[4]

[1]U.S. Department of Energy, National Energy Technology Laboratory, 3610 Collins Ferry Road, Morgantown, WV 26507

[2]U.S. Department of Energy, Oak Ridge Institute for Science and Education (ORISE), 3610 Collins Ferry Road, Morgantown, WV 26507

[3]NETL Support Contractor, 3610 Collins Ferry Road, Morgantown, WV 26507

[4]Kansas Geological Survey, University of Kansas, Lawrence, 1930 Constant Avenue, Lawrence, KS 66047

DOE/NETL-2022/3725

21 January 2022

NETL Contacts:

Dustin Crandall, Principal Investigator and Technical Portfolio Lead

Bryan Morreale, Executive Director, Research & Innovation Center

This page intentionally left blank.

Table of Contents

This page intentionally left blank.

List of Figures

List of Figures (cont.)

List of Figures (cont.)

List of Tables

This page intentionally left blank.

Acronyms, Abbreviations, and Symbols

Term	Description
2D	Two-dimensional
3D	Three-dimensional
CO_2	Carbon dioxide
CT	Computed tomography
CTN	CT number
DOE	Department of Energy
EDX	NETL's Energy Data eXchange
HU	Hounsfield Unit
KGS	Kansas Geological Survey
MSCL	Multi-Sensor Core Logger
NETL	National Energy Technology Laboratory
ORISE	Oak Ridge Institute for Science and Education
XRF	X-ray fluorescence

Acknowledgments

This work was completed at the National Energy Technology Laboratory (NETL) with support from U.S. Department of Energy's (DOE) Office of Fossil Energy Oil & Gas Program. The authors wish to acknowledge Bryan Morreale (NETL Research & Innovation Center), Mark McKoy (NETL Technology Development and Integration Center), and Darin Damiani (DOE Office of Fossil Energy) for programmatic guidance, direction, and support.

The authors would like to thank Scott Workman and Bryan Tennant for computed tomography data collection and technical support. Thank you to the staff of the Geologic Characterization, Analytics and Modeling laboratory for continued laboratory support. This research was supported in part by appointments from the NETL Research Participation Program, sponsored by the U.S. DOE and administered by the Oak Ridge Institute for Science and Education (ORISE).

ABSTRACT

The computed tomography (CT) facilities and the Multi-Sensor Core Logger (MSCL) at the National Energy Technology Laboratory (NETL) in Morgantown, West Virginia were used to characterize core from the Wellington KGS 2-32 well (API 15-191-22770). Core from the well was obtained as part of the Small-Scale Field Test Demonstrating Carbon Dioxide (CO_2) Sequestration in Arbuckle Saline Aquifer and by CO_2-Enhanced Oil Recovery at Wellington Field, Sumner County, Kansas (DE-FE0006821).

The primary impetus of this work was to capture a detailed a digital representation of the core from the Wellington KGS 2-32 well (Sumner County, Kansas). The collaboration between the U.S. Department of Energy's (DOE) NETL and the Kansas Geological Survey (KGS) at the University of Kansas enables other research entities to access information about this potential carbon storage location and formations. The resultant datasets are presented in this report and can be accessed from NETL's Energy Data eXchange (EDX) online system using the following link: https://edx.netl.doe.gov/dataset/wellington2-32-core.

All equipment and techniques used were non-destructive, enabling future examinations and analyses to be performed on these cores. Fractures, discontinuities, and millimeter-scale features were readily detectable with the medical CT scanner-acquired images. Imaging with the NETL medical CT scanner was performed on the entire core. Qualitative analysis of the medical CT images, coupled with X-ray fluorescence, P-wave, gamma density, and magnetic susceptibility measurements from the MSCL were useful in identifying zones of interest for more detailed analysis. Higher-resolution industrial CT images were acquired of selected zones along the depth of the core to visualize the structure in higher detail. The ability to quickly identify key areas for more detailed study with higher resolution will save time and resources in future studies. The combination of methods used provides a multi-scale analysis the core; the resulting macro- and micro-descriptions are relevant to many subsurface energy related examinations traditionally performed at NETL.

1. INTRODUCTION

Evaluation of reservoir samples can support resource estimations for geologic carbon dioxide (CO_2) storage. While it is common for commercial entities to perform these characterizations, the resources necessary to conduct these analyses are not always available to the broader interest base, such as state agencies and research-based consortia. To meet the growing need for comprehensive and high-quality lithologic data for collaborative research initiatives, the U.S. Department of Energy's (DOE) National Energy Technology Laboratory (NETL) has used available resources to develop a systematic approach for the evaluation of subsurface geological core materials.

In this study, the primary objective was to characterize core with methods not available to most researchers. The data is presented in several formats here and online from NETL's Energy Data eXchange (EDX) (https://edx.netl.doe.gov/dataset/wellington2-32-core) are potentially useful for various analyses. However, little detailed analysis is presented in this report as the research objective was not to perform a site characterization, but rather to acquire the data for others to utilize and to create a digital representation of the core that could be preserved in perpetuity. A lengthy and robust core analysis was performed by Kansas Geological Survey (KGS) as part of the DOE funded project DE-FE0006821 (Watney et al., 2017; Holubnyak et al., 2017) that can be reviewed for a more complete understanding of the formations of interest in the Wellington Field.

1.1 SITE BACKGROUND

Wellington KGS 2-32 was drilled in association with Small Scale Field Test Demonstrating CO_2 Sequestration in Arbuckle Saline Aquifer and by CO_2-Enhanced Oil Recovery at Wellington Field (DE-FE0006821) near the town of Wellington, Sumner County, Kansas. The Wellington Field produced 20 million barrels of oil over 26 years (1929–1957). primarily from Mississippian age reservoirs, before being transitioned to a tertiary waterflood recovery field in 1957 (Holubnyak et al., 2017). In 2020, it produced approximately 40,392 barrels of oil (~100 barrels per day) and 20,950,498 mcf of natural gas from 49 active production wells and 15 injection wells (KGS, 2021).

The Wellington KGS 2-32 well (API 15-191-22770) was drilled as a CO_2 injection well to a depth of 3,860 ft in March 2015, targeting the Mississippian Limestone. The well was cored from 3,654–3,752 ft which encompasses rock from the bottom 6 ft of the superjacent Cherokee Group through the entire Mississippian Lime reservoir interval.

1.2 GEOLOGIC BACKGROUND

The Wellington KGS 2-32 well sits on the eastern edge of the Sedgwick Basin, which is dominated by carbonate sediments deposited in a shallow marine environment during the Mississippian. The Sedgwick Basin is bordered to the west by the Pratt Anticline and Central Kansas Uplift, to the north by the Salina Basin, and west by the Nemaha Ridge. Dynamic sea level rise and fall led to deposition of interbeds of lime-rich mud, shell-debris and chert. The Nehama Ridge, which uplifts the underlying Precambrian basement, experienced significant movement during the Pennsylvanian, which lead to weathering portions of Mississippian Lime. The weathered portions contain vug-rich "chat" zones and many of the stratigraphic traps in the Wellington Field (Watney et al., 2002; Evans and Newell, 2013).

The Mississippi Lime in the study area is primarily made up of the Cowley facies. The Cowley is a cherty, fine-grained limestone with some interbedded shale (Evans and Newell, 2013). The top of Mississippian deposition is expected to be found at a depth of approximately ~2,500 ft above mean sea level and the Cowley Formation itself is ~250 ft thick (Figure 1 and Figure 2, respectively) (KGS, 1998).

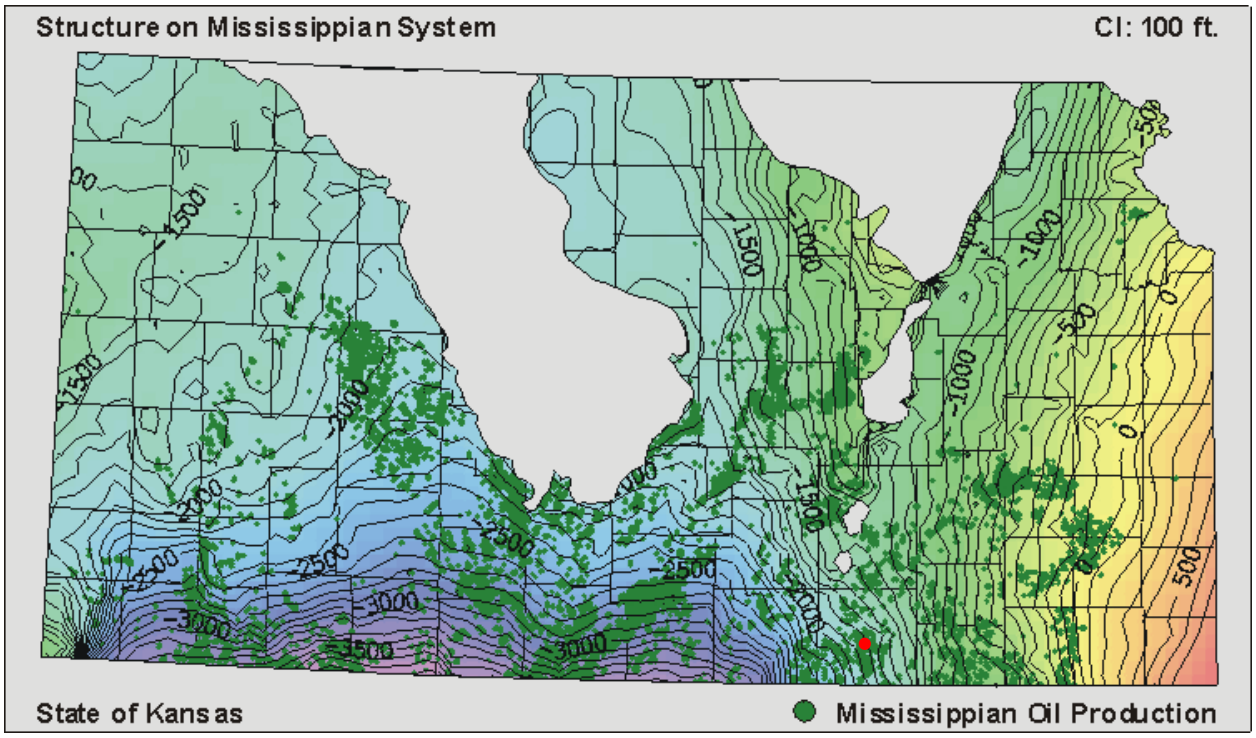

Figure 1: Mississippian System structure map with Wellington KGS 2-32 well represented by the red point and oil fields in green (modified from KGS, 1998).

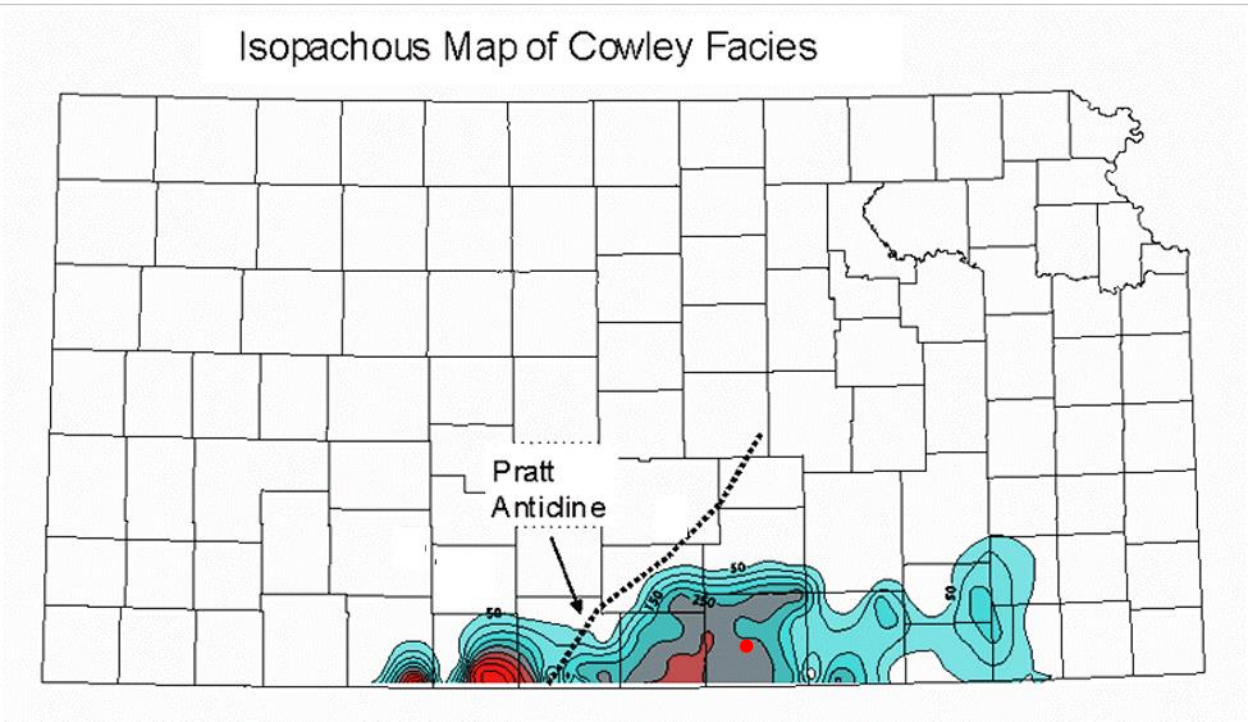

Figure 2: Cowley Facies isopach map with the red dot representing Wellington KGS 2-32 (modified from Watney et al., 2002)

1.3 CORE DESCRIPTION

Wellington KGS 2-32 was cored from the base of the superjacent Cherokee Group through the Upper Mississippian series, which is made up of primarily dolomite and dolomitic limestone with intervals of chert and vugs. There is a decrease in chert content and vugs, and an increase in argillaceous dolomites, with increasing depth. The upper part of the Upper Mississippian Series, known colloquially as the Mississippi Lime or Mississippi "Chat", is primarily made up of polymictic chert breccia with some sucrosic dolomite reworked throughout and is approximately 20-ft thick. The Cherokee Group is made of a variety of lithologies, primarily mudstone and paleosols (Scheffer, 2012). The bottom 6 ft of the Cherokee recovered in the well is made up of shale with some minor intervals of paleosols and chert nodules. Figure 3 provides a detailed lithology description of the Wellington KGS 2-32 well from the Kansas Geological Survey (KGS, 2015, link).

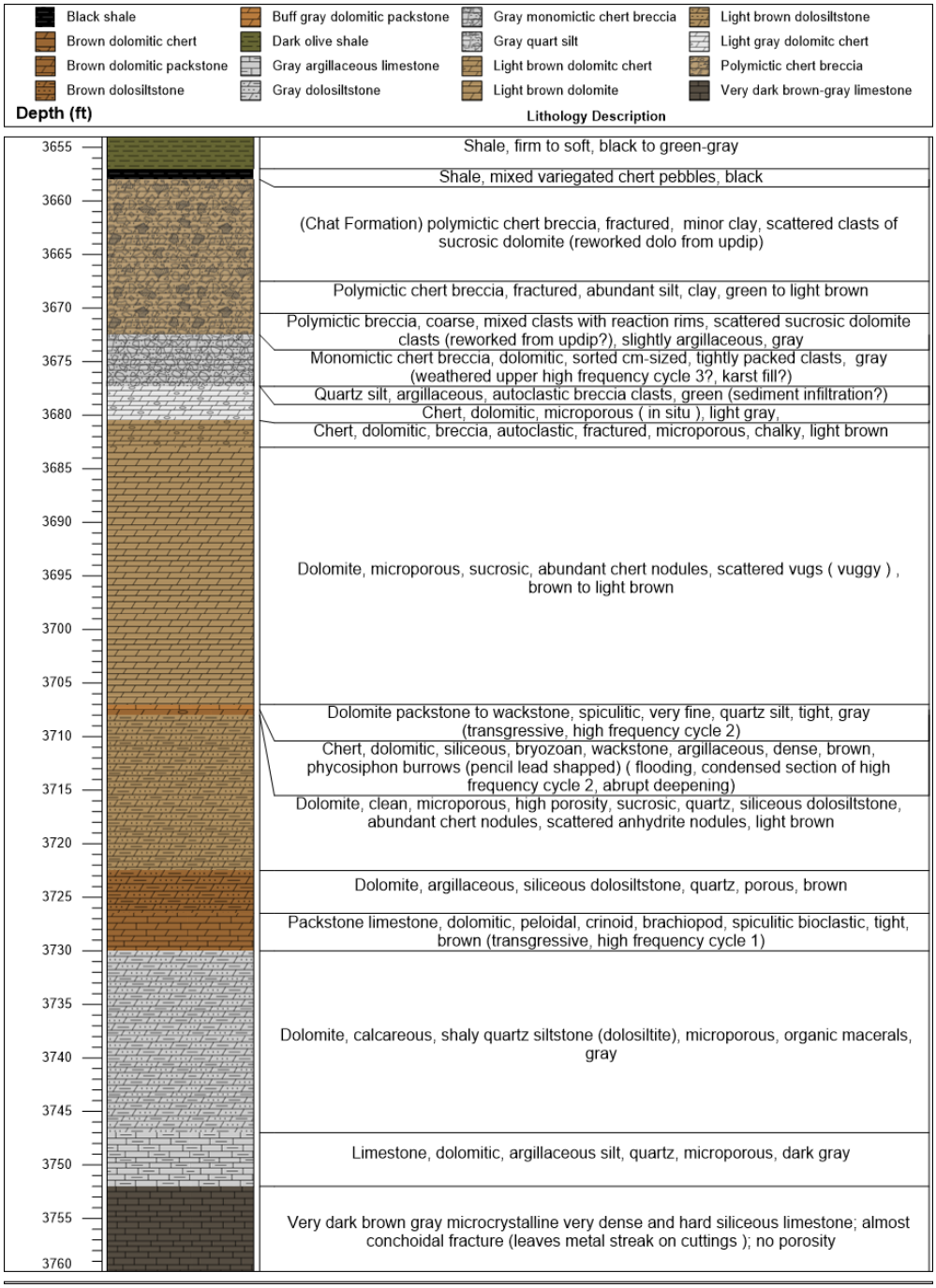

Figure 3: Description of cored interval (3,654–3,760 ft), evaluated by Kansas Geological Survey, compiled by Thomas Paronish.

1.4 CORE PHOTOGRAPHS

Figures 4 through 15 represent core photos of the Wellington KGS 2-32, 4-in. diameter whole core. High resolution photos are available on the KGS website (KGS, 2015, link).

3,654–3,657 ft **3,657–3,660 ft** **3,660–3,663 ft**

Figure 4: Wellington KGS 2-32 core photos from 3,654–3,663 ft.

3,663–3,666 ft **3,666–3,669 ft** **3,669–3,670.8 ft**

Figure 5: Wellington KGS 2-32 core photos from 3,663–3,670.8 ft.

3,670.8–3,673.8 ft **3,673.8–3,676.8 ft** **3,676.8–3,679.8 ft**

Figure 6: Wellington KGS 2-32 core photos from 3,670.8–3,679.8 ft.

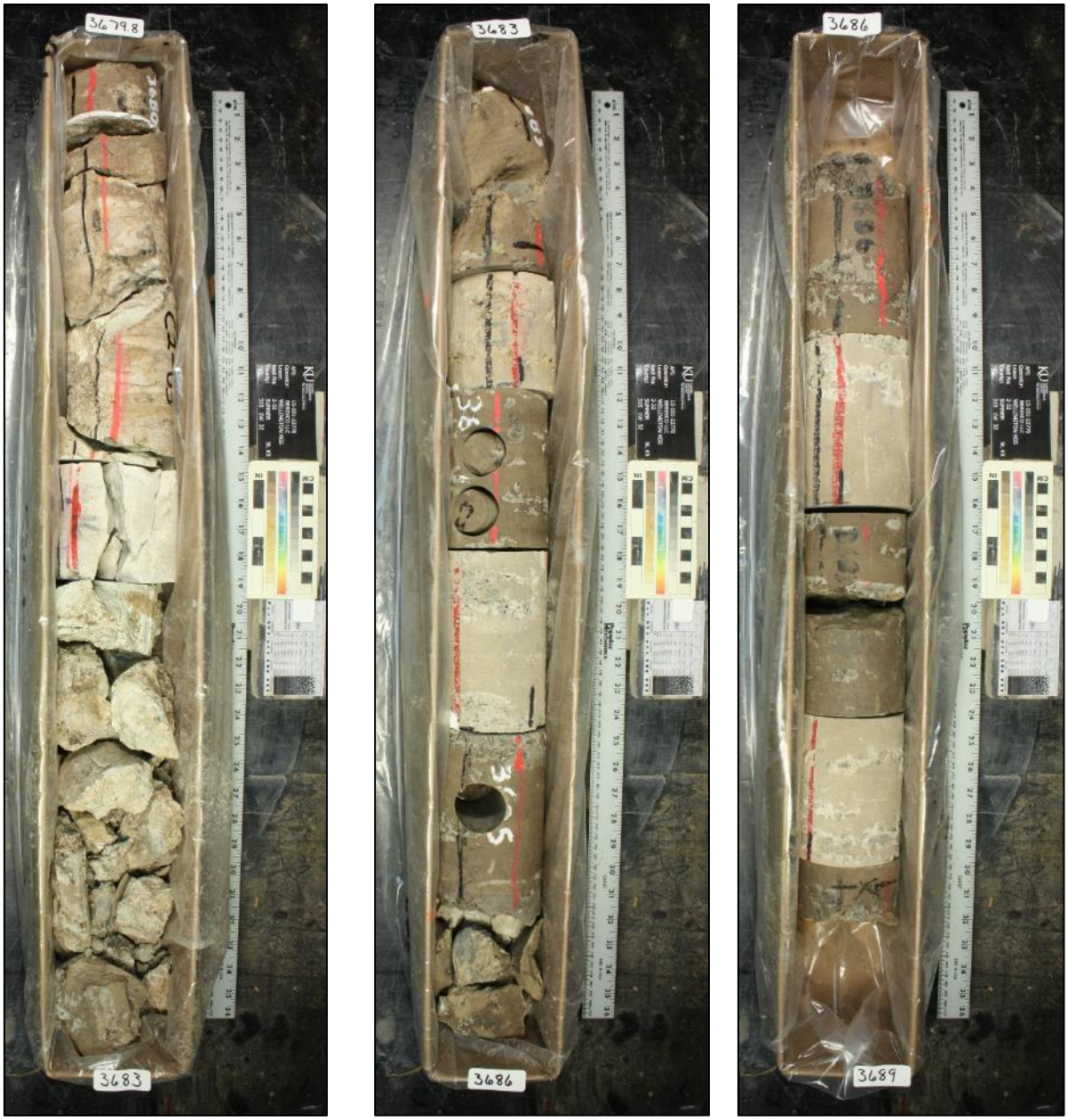

3,679.8–3,683 ft **3,683–3,686 ft** **3,686–3,689 ft**

Figure 7: Wellington KGS 2-32 core photos from 3,679.8–3,689 ft.

3,688.2–3,691.2 ft **3,691.2–3,693.5 ft** **3,693.5–3,696.4 ft**

Figure 8: Wellington KGS 2-32 core photos from 3,688.2–3,696.4 ft.

3,696.4–3,699 ft **3,699–3,701.5 ft** **3,701.5–3,703.75 ft**

Figure 9: Wellington KGS 2-32 core photos from 3,696.4–3,703.75 ft.

3,703.75–3,707 ft **3,707–3,708.55 ft** **3,708.55–3,711.55 ft**

Figure 10: Wellington KGS 2-32 core photos from 3,703.75–3,711.55 ft.

3,711.55–3,714.7 ft **3,714.7–3,717.6 ft** **3,717.6–3,720.6 ft**

Figure 11: Wellington KGS 2-32 core photos from 3,711.55–3,720.6 ft.

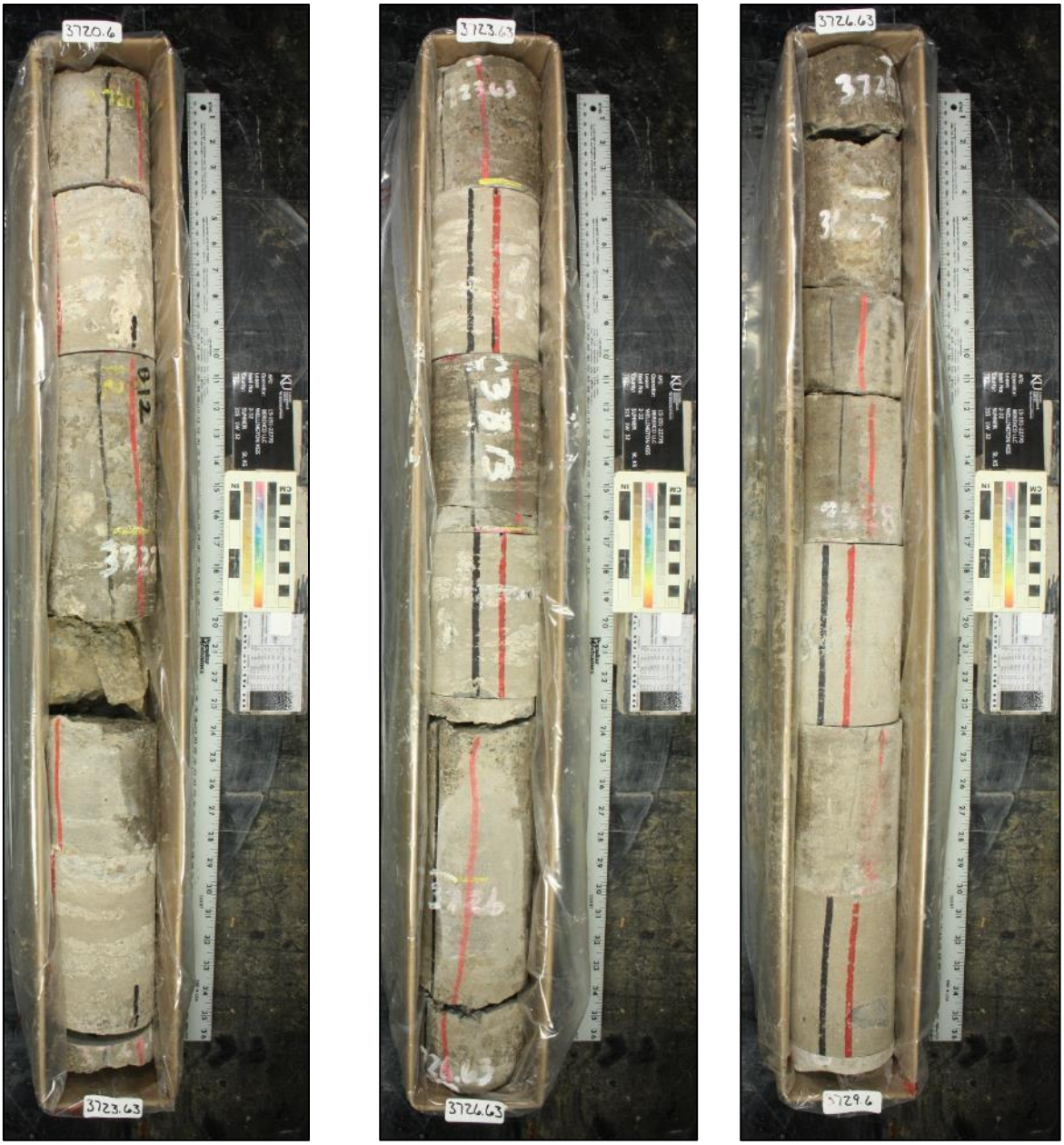

3,720.6–3,723.63 ft **3,723.63–3,726.63 ft** **3,726.63–3,729.6 ft**

Figure 12: Wellington KGS 2-32 core photos from 3,720.6–3,729.6 ft.

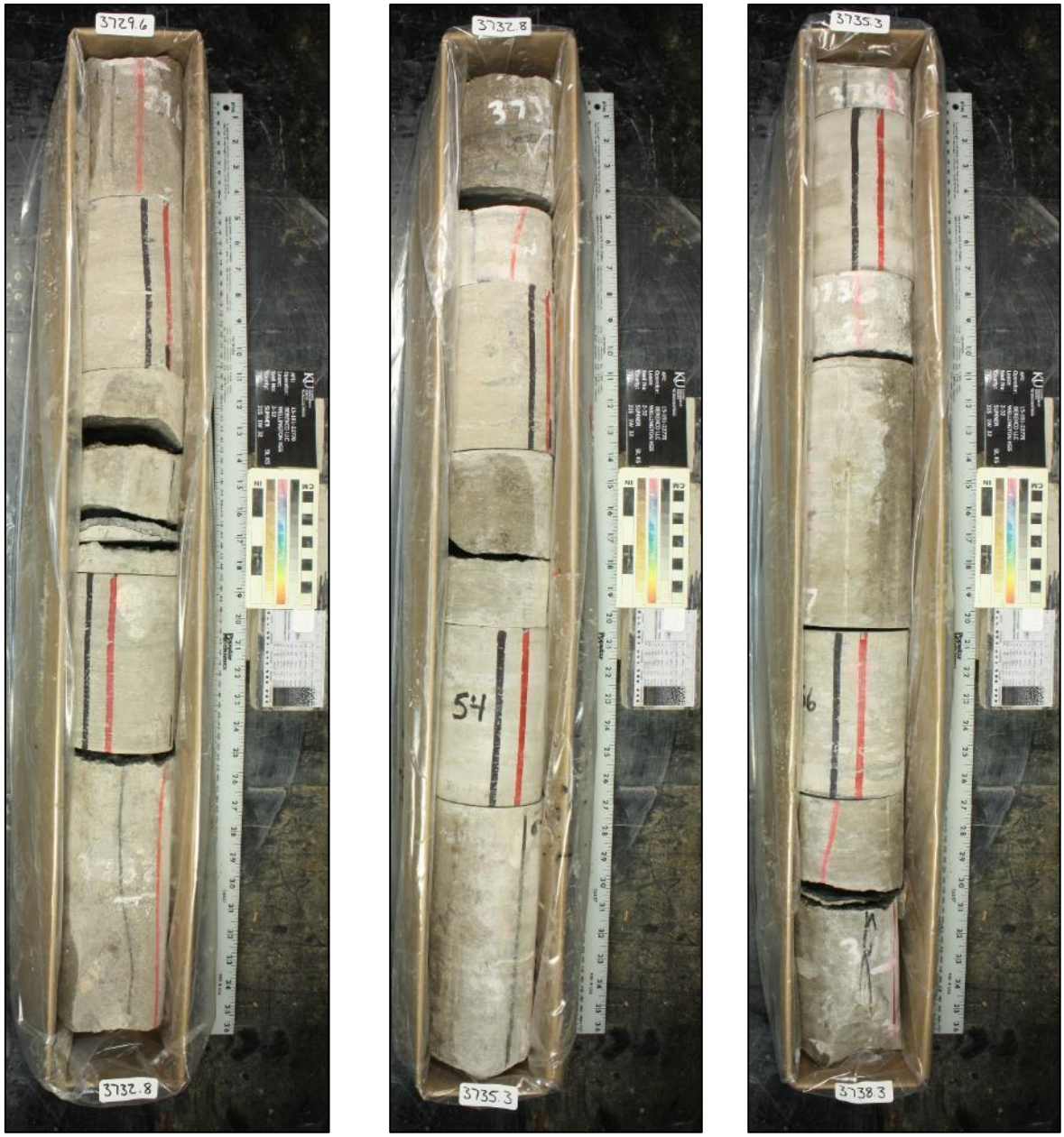

3,729.6–3,732.8 ft **3,732.8–3,735.3 ft** **3,735.3–3,738.3 ft**

Figure 13: Wellington KGS 2-32 core photos from 3,729.6–3,738.3 ft.

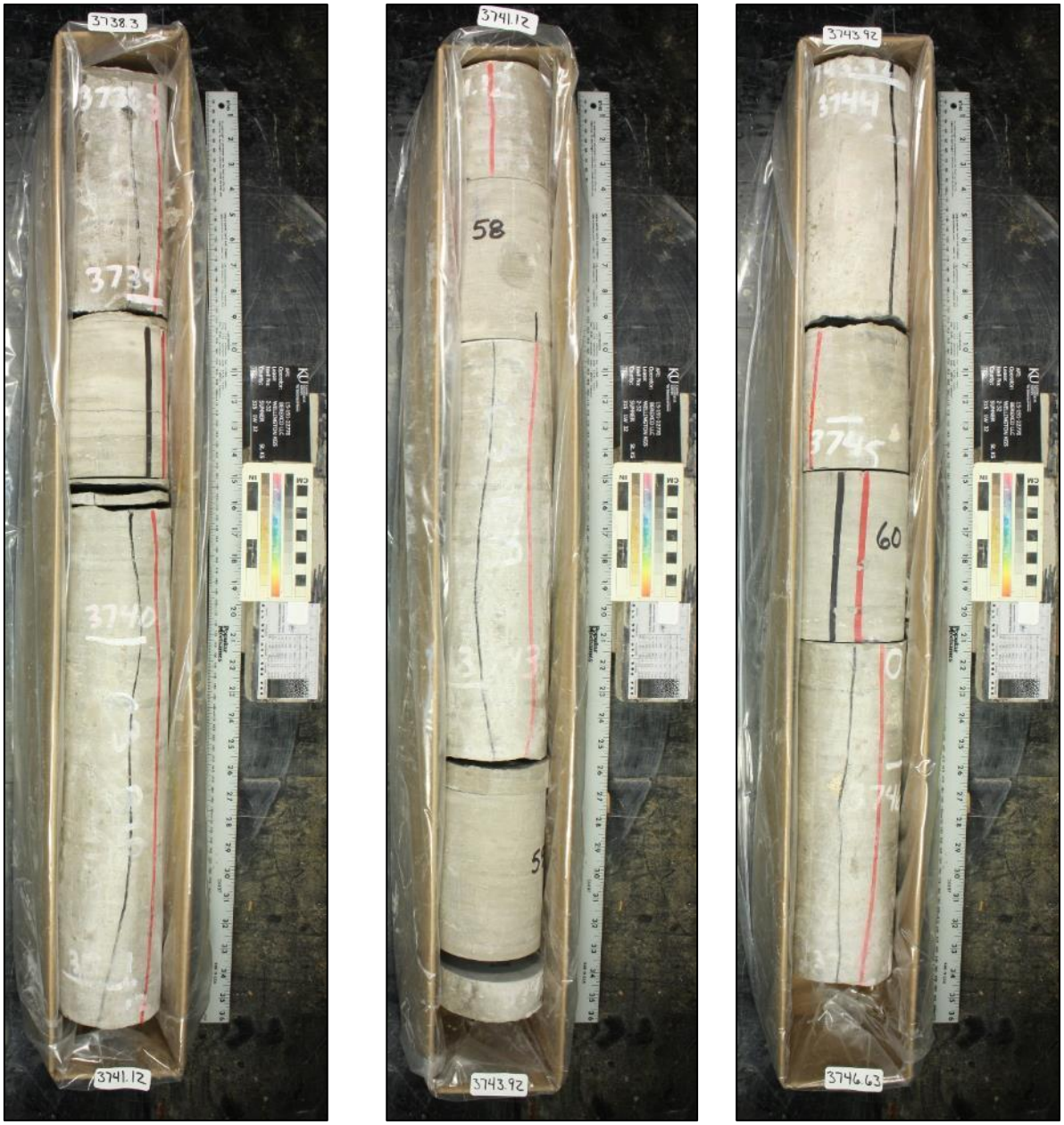

3,738.3–3,741.12 ft **3,741.12–3,743.92 ft** **3,743.92–3,746.63 ft**

Figure 14: Wellington KGS 2-32 core photos from 3,738.3–3,746.63 ft.

3,746.63–3,749.1 ft

3,749.1–3,752.08 ft

Figure 15: Wellington KGS 2-32 core photos from 3,746.63–3,752.08 ft.

2. DATA ACQUISITION AND METHODOLOGY

The core was evaluated using medical-grade computed tomography (CT) scanning and high spatial resolution geophysical measurements along its length, including X-ray fluorescence (XRF) spectrometry.

2.1 MEDICAL CT SCANNING

Core scale CT scanning was performed with a Toshiba Aquilion TSX-101A/R medical CT scanner as shown in Figure 16. The medical CT scanner generates images with a resolution in the millimeter range, with scans having voxel resolutions of 0.43 x 0.43 mm in the XY plane and 0.50 mm along the core's long axis (i.e., z-axis). The scans were conducted at a voltage of 135 kV and at a current of 200 mA. Subsequent processing and combining of stacks were performed to create three-dimensional (3D) volumetric representations of the cores and a two-dimensional (2D) cross-section through the middle of the core samples using ImageJ (Schneider, 2012). The variation in greyscale values observed in the CT images indicates changes in the CT number (CTN) obtained from the CT scans, which is directly proportional to changes in the attenuation and density of the scanned rock. Darker regions are less dense. As can be seen in Figure 21 through Figure 32, filled fractures, open fractures, and changes in bedding structure can all be resolved via careful examination of the CT images. While the medical CT scanner was not used for detailed characterization in this study, it allowed for non-destructive bulk characterization of the core.

Figure 16: Toshiba Aquilion Multislice Helical CT scanner at NETL used for core analysis.

2.2 CORE LOGGING

Geophysical measurements of P-wave travel time, magnetic susceptibility, and attenuated gamma counts were obtained with a Geotek® Multi-Sensor Core Logging (MSCL) system on a competent core. For the Wellington KGS 2-32 core the P-wave velocity, attenuated gamma counts, and magnetic susceptibility were measured and are reported (Figure 46 and Figure 47). Additionally, the system was used to measure bulk elemental chemistry with a built-in, portable XRF spectrometer. The compiled core logs were scaled to fit on single pages for rapid review of the combined data from the medical CT scans and XRF readings. Core scale CT scanning was done with a Toshiba Aquilion TSX-101A/R medical CT scanner.

2.2.1 Magnetic Susceptibility

Magnetic susceptibility is a measure of the degree of magnetization in a sample. The sample is exposed to an external magnetic field and magnetic susceptibility is its measured magnetic response to that field:

$$J = kH$$

Where, J is the magnetic response (per unit volume), k is volume susceptibility, and H is an external magnetic field. The measurement unit is dimensionless (abbreviated simply as SI).

All materials have magnetic susceptibility. Positive values of magnetic susceptibility indicate that materials are *paramagnetic* and occur in rocks that consist of the majority ferromagnetic, ferrimagnetic, or antimagnetic (iron-bearing) materials. Negative values of magnetic susceptibility indicate that materials are *diamagnetic* and occur in rocks dominated by non-iron material (e.g., calcite or quartz). Table 1 lists examples of common magnetic susceptibility ranges (Hunts et al., 1995).

Magnetic susceptibility was measured using the Bartington point sensor, where a 1-cm diameter, low intensity (8.0 A/m RMS), non-sensitive, alternating magnetic field (2 kHz) was generated for 10 s. To minimize any potential drift in the oscillating field, the point sensor was zeroed at the beginning and end of the sample and after every 5th measurement. The point sensor due to the small field, was limited in whole core measurements, and additionally was temperature dependent (Geotek Ltd. Multi-Sensor Core Logger Manual, Version 05-10; Geotek Ltd., 2010).

Table 1: Magnetic Susceptibility Values for Common Minerals (Hunts et al., 1995)

Mineral	x (*10^{-6}) SI
Water	9
Calcite	-7.5 to -39
Halite, Gypsum	-10 to -60
Shale	63 to 18,600
Illite, Montmorillonite	330 to 410
Pyrite	5 to 3,500
Chalcopyrite	23 to 400
Hematite	500 to 40,000
Magnetite	1,000,000 to 5,700,000

2.2.2 P-wave Velocity

P-wave velocity measurements were performed to measure the acoustic impedance of a geologic sample with respect to compressional waves. Acoustic impedance is a measure of how well a material transmits vibrations, which is directly proportional to the material's density or consolidation. An example of a material that has a high acoustic impedance would be air, with a P-wave speed of 330 m/s. Granite has a low acoustic impedance, with a wave speed of over 5,000 m/s. These measurements can be proxies for seismic reflection coefficients and can be translated to field use when performing seismic surveys.

The software associated with the MSCL measures the travel time of the pulse with a resolution of 50 ns. The absolute accuracy of the instrument measurements is ± 3 m/s with a resolution of 1.5 m/s (Geotek Ltd. Multi-Sensor Core Logger Manual, Version 05-10; Geotek Ltd., 2010).

2.2.3 Gamma Density

Gamma density was acquired by subjecting the sample to gamma radiation and then measuring the attenuation of that radiation. The attenuation is directly proportional to the density of the sample and is acquired by measuring the difference between radiation energy at the emission source and after it passes through the sample. Specifically, the MSCL software calculates the bulk density, ρ, by using the following equation:

$$\rho = \left(\frac{1}{\mu d}\right) \ln\left(\frac{I_o}{I}\right)$$

Where μ = Compton attenuation coefficient, d = sample thickness, I_o = source intensity, and I = measured intensity.

2.2.4 X-ray Fluorescence Spectrometry

In addition to the geophysical measurements a portable, handheld Innov-X® XRF Spectrometer was used to measure relative elemental abundances. The Mining-Plus Suite of the Innov-X® handheld XRF Spectrometer was utilized at 6 cm resolution with 60 s exposure time per beam. The Mining-Plus Suite utilizes a 2-beam analysis that resolves major elements (Mg, Al, Si, P, S, Cl, Fe, K, Ca, and Ti), minor elements (V, Cu, Ni, Cr, Mn, and Pb), trace elements (Co, Zn, As, Zr, Mo, Ag, Cd, Sn, Sb, Hf, W, and Bi) and an aggregated "light element" (H to Na) (Figure 17). Elemental abundances are reported relative to the total elemental composition (i.e., out of 100% weight).

The XRF spectrometer measures elemental abundances by subjecting the sample to X-ray photons. The high energy of the photons displaces inner-orbital electrons in the respective elements. The vacancies in the lower orbitals cause outer-orbital electrons to "fall" into lower orbits to satisfy the disturbed electron configuration. The substitution into lower orbitals causes a release of a secondary X-ray photon, which has an energy associated with a specific element. These relative and element specific energy emissions can then be used to determine bulk elemental composition.

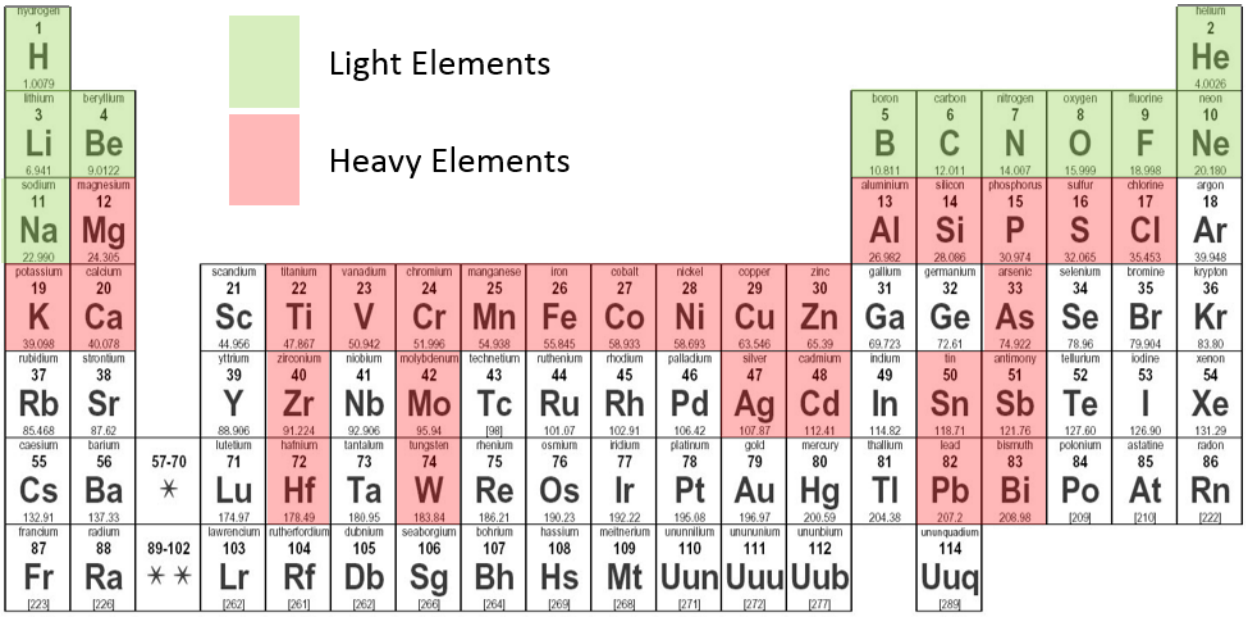

Figure 17: Periodic table showing elements measurable by the Innov-X® XRF Spectrometer using the Mining-Plus.

2.3 HIGH RESOLUTION INDUSTRIAL CT SCANNING

Selected cores from the Wellington KGS 2-32 well were scanned using NETL's NorthStar Imaging Inc. M-5000® Industrial CT System (Industrial CT) (Figure 18). The scan on sections of the whole core were performed at a voltage of 185 kV and a current of 200 µA. A 2 x 2 pixel binning on the Perkin Elmer detection panel was performed to reduce noise and scatter. These settings provided the proper photon energy to penetrate the samples. The samples were rotated 360° and 1,440 radiograph projections of the samples were obtained, averaging 10 individual radiographs at each step to create the reconstruction. These scan settings resulted in high resolution scans with voxel resolutions between 58 and 67 μm^3 (Table 4).

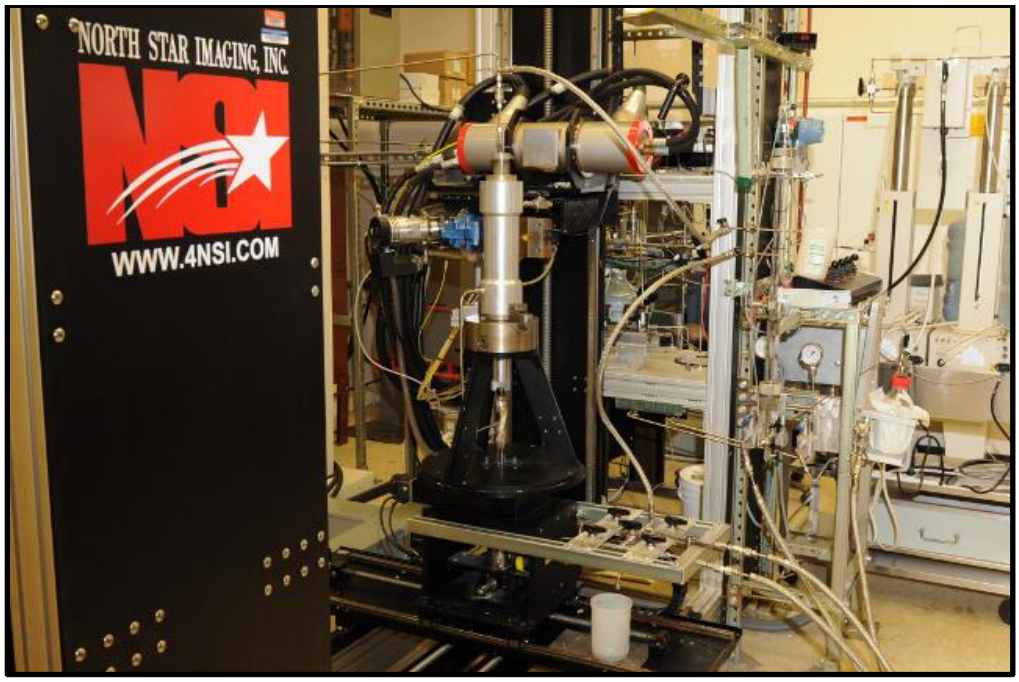

Figure 18: North Star Imaging Inc. M-5000 ® Industrial CT Scanner at NETL.

2.4 DATA COMPILATION

Strater® by Golden Software was used to compile the medical CT data into a series of logs. The data used to generate these logs can be accessed from NETL's EDX online system using the following link: https://edx.netl.doe.gov/dataset/wellington2-32-core.

3. RESULTS

The following section contains the data obtained from the medical CT and the MSCL scans of the core obtained from Wellington KGS 2-32 well.

3.1 MEDICAL CT SCANS

Processed 2D slices of the medical CT scans through the cores are shown first, followed by various analyses of fractures and variations in the shale structure observed from the medical CT scans. As discussed previously, the variation in greyscale values observed in the medical CT images indicates changes in the CTN obtained, which is directly proportional to changes in the attenuation of the X-ray beam and thus density of the scanned rock (i.e., darker regions are less dense, lighter regions are denser).

Core was scanned in 3 ft or smaller sections. Detailed information in logbooks and photographs of the core were used to confirm the locations of missing core and depths.

3.1.1 X/Z Planes

A 2D image through the center of each core can be found in Figure 21 through Figure 32 (on the left of each column). These are referred to as "XZ" planes with the coordinates that are shown in Figure 19. There is no scale bar shown in these images; the core has a diameter of 4 in. (10.16 cm) for reference. The labels below each 2D XZ plane in Figure 21 through Figure 32 are the depth at the bottom of each core; the full range of core lengths shown in each figure is listed in the figure captions. The greyscale values were shifted in these images to best represent the structure of the core in each image.

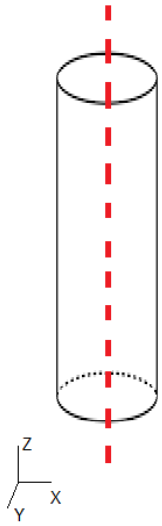

Figure 19: Schematic of the XZ isolated plane through the vertical center of the medical CT scans.

3.1.2 Polar Transform

A 2D image through the circumference of the core can be found in Figure 21 through Figure 32 (on right of each column). There images are referred to as "Polar Transform" images. The original XY CT image is "unwrapped" from polar coordinates to a cartesian coordinates where, the y-axis represents the angle from 0 to 360° and the x-axis represents the distance from the center of the image (Figure 20). This is done for all slices in the volume. The resulting volume is resliced perpendicular to the XY plane and an isolated plane is taken along the outer most portion of the core.

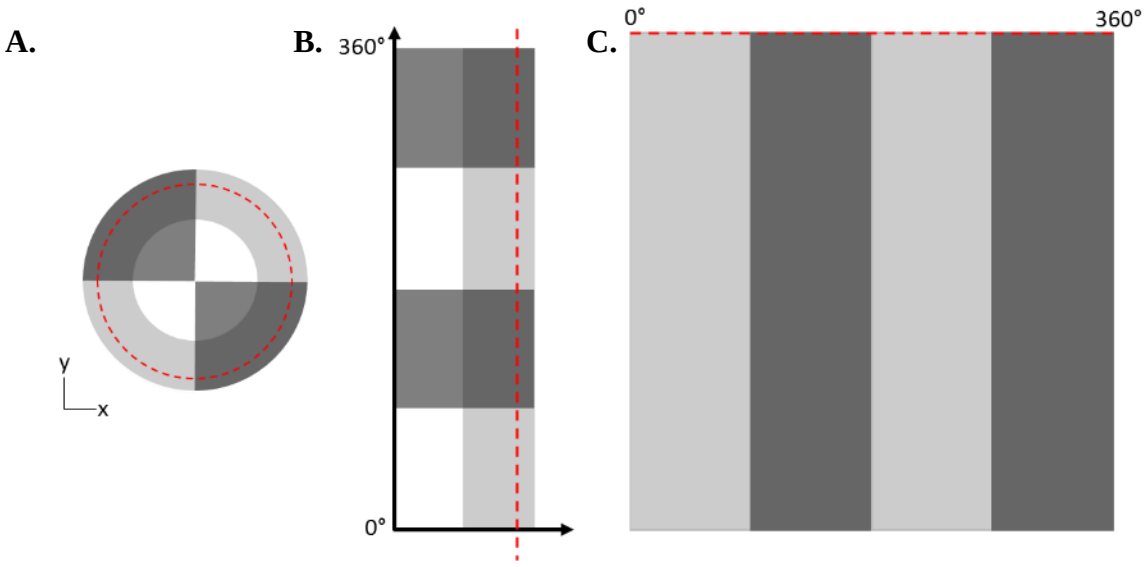

Figure 20: Schematic of the polar transform isolated plane around the circumference of the medical CT scans; (A) original CT image slice, (B) cartesian "remapping" image, (C) Polar transform image

3.2 WELLINGTON KGS 2-32 CORE SAMPLES

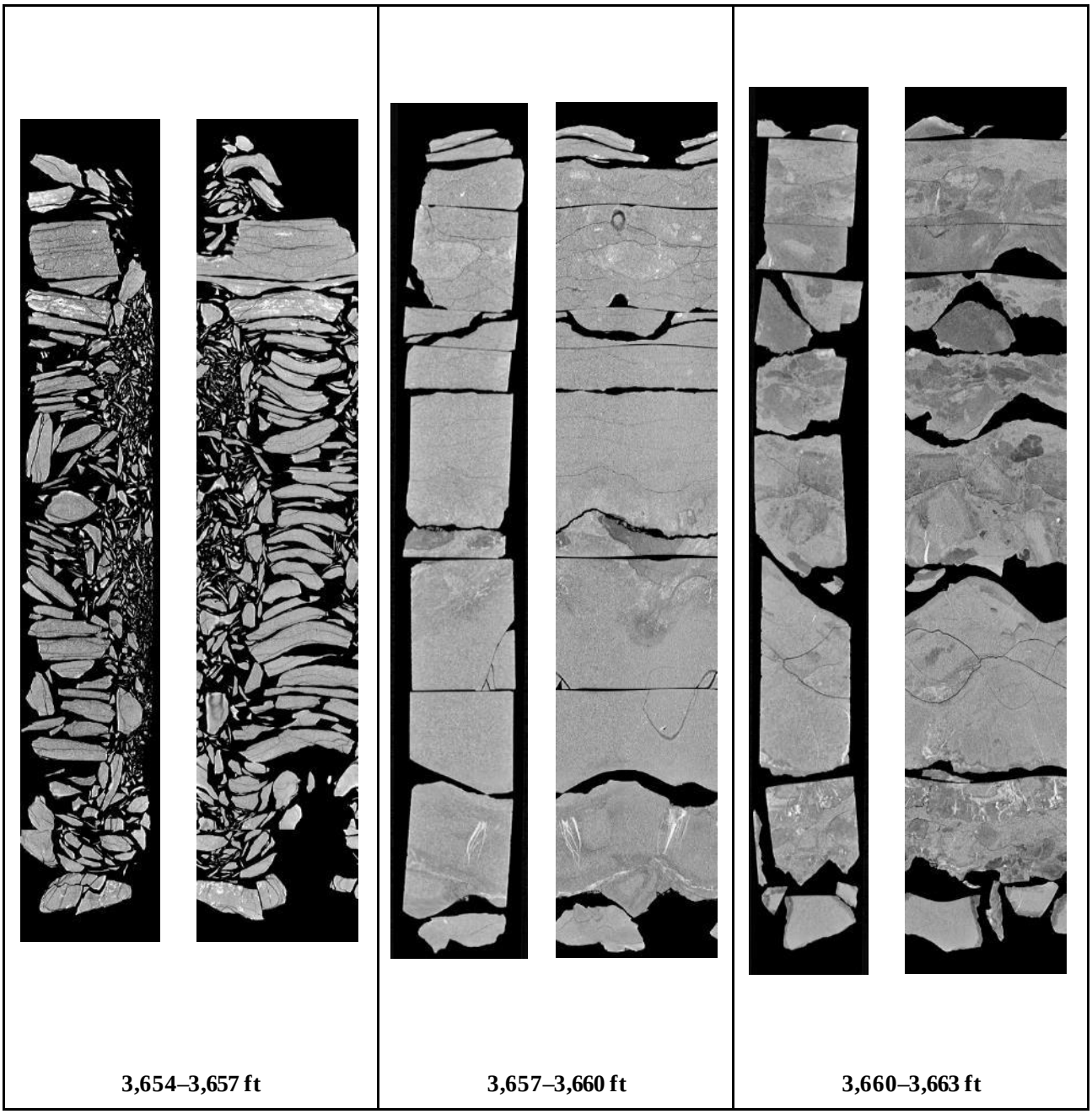

Figure 21: 2D isolated planes through the vertical center and a polar transform of the outside of the medical CT scans of Wellington KGS 2-32 core from 3,654.0–3,663 ft.

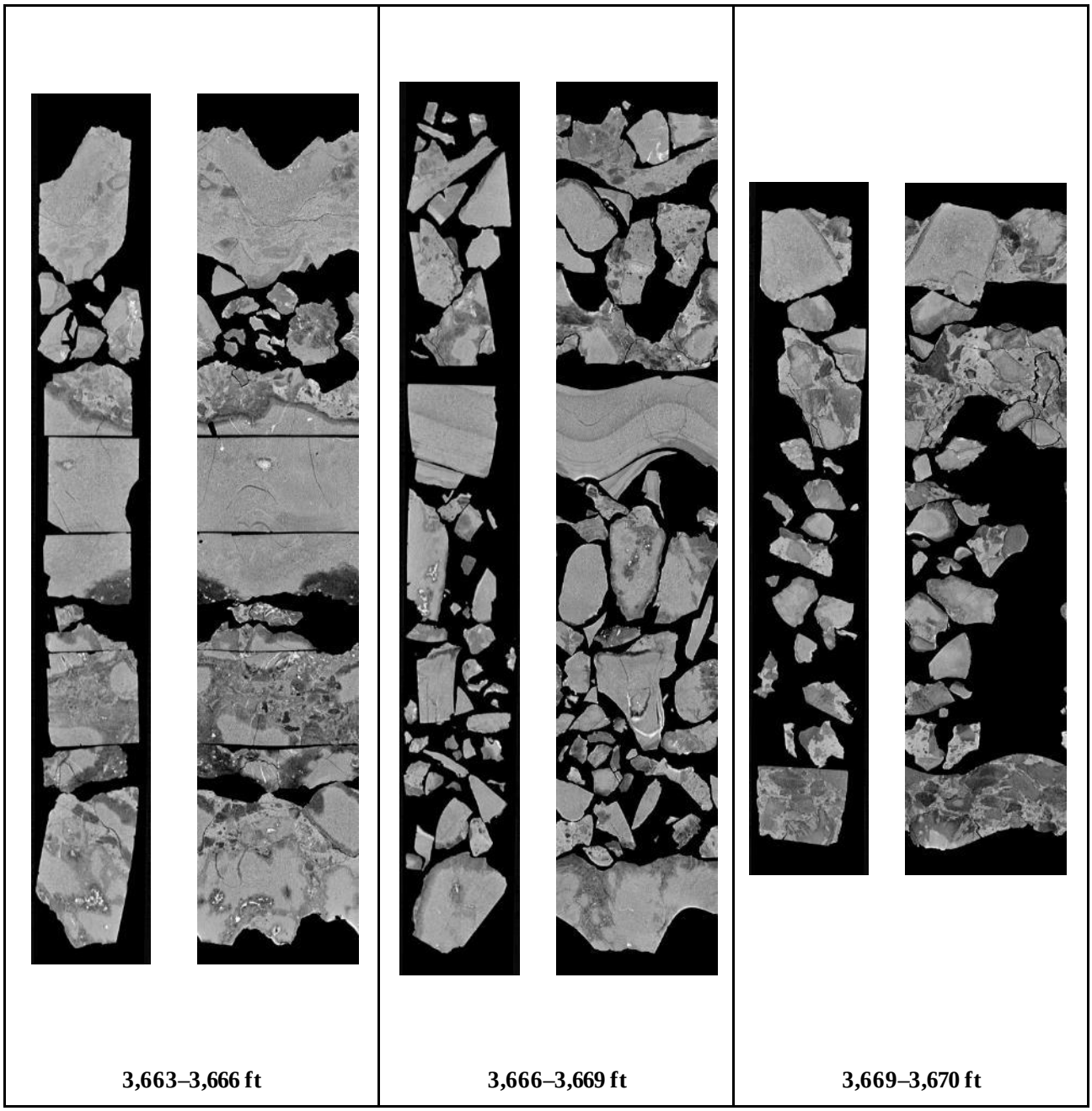

Figure 22: 2D isolated planes through the vertical center and a polar transform of the outside of the medical CT scans of Wellington KGS 2-32 core from 3,663–3,670 ft.

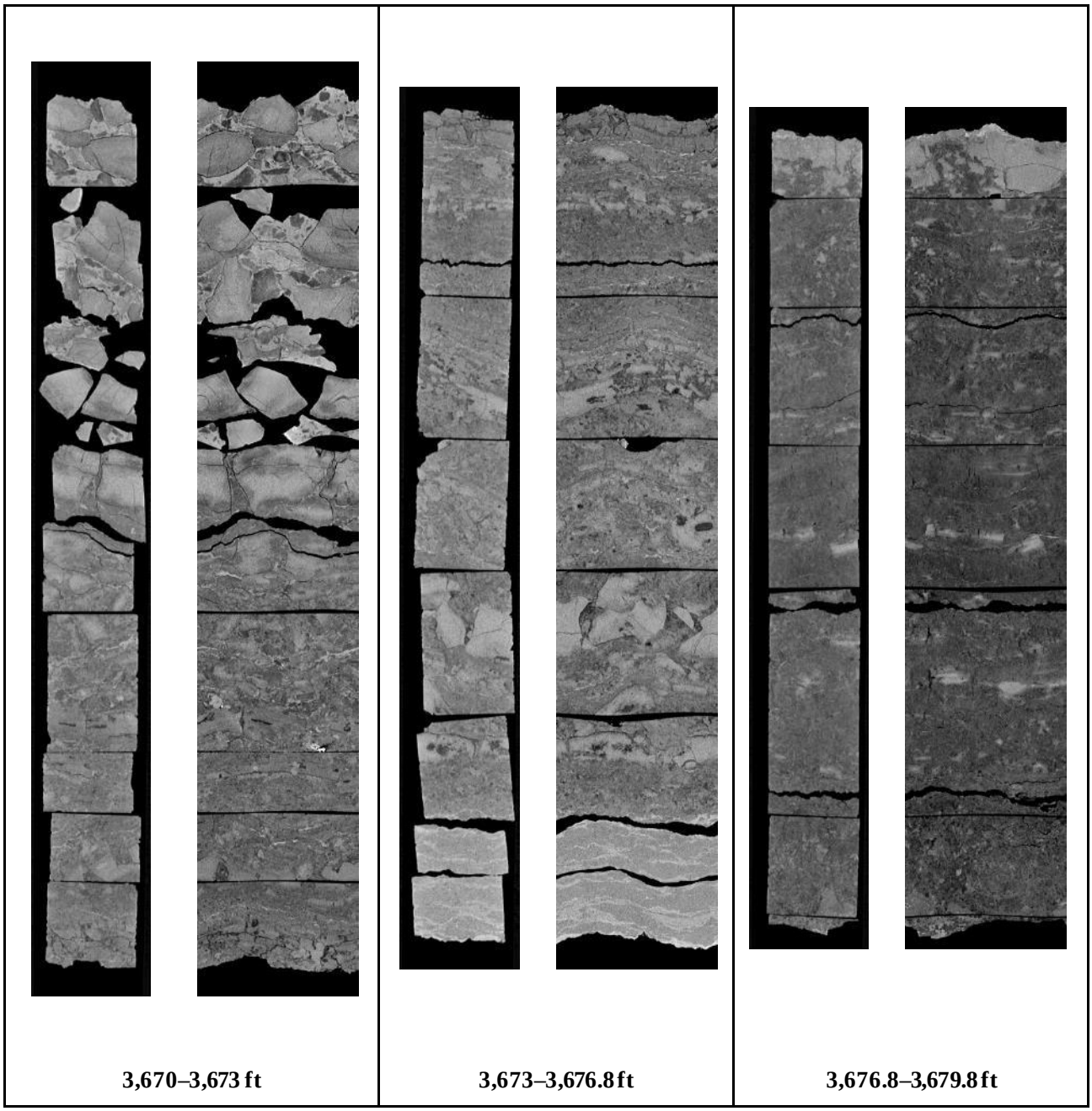

Figure 23: 2D isolated planes through the vertical center and a polar transform of the outside of the medical CT scans of Wellington 2-32 core from 3,670–3,679.8 ft.

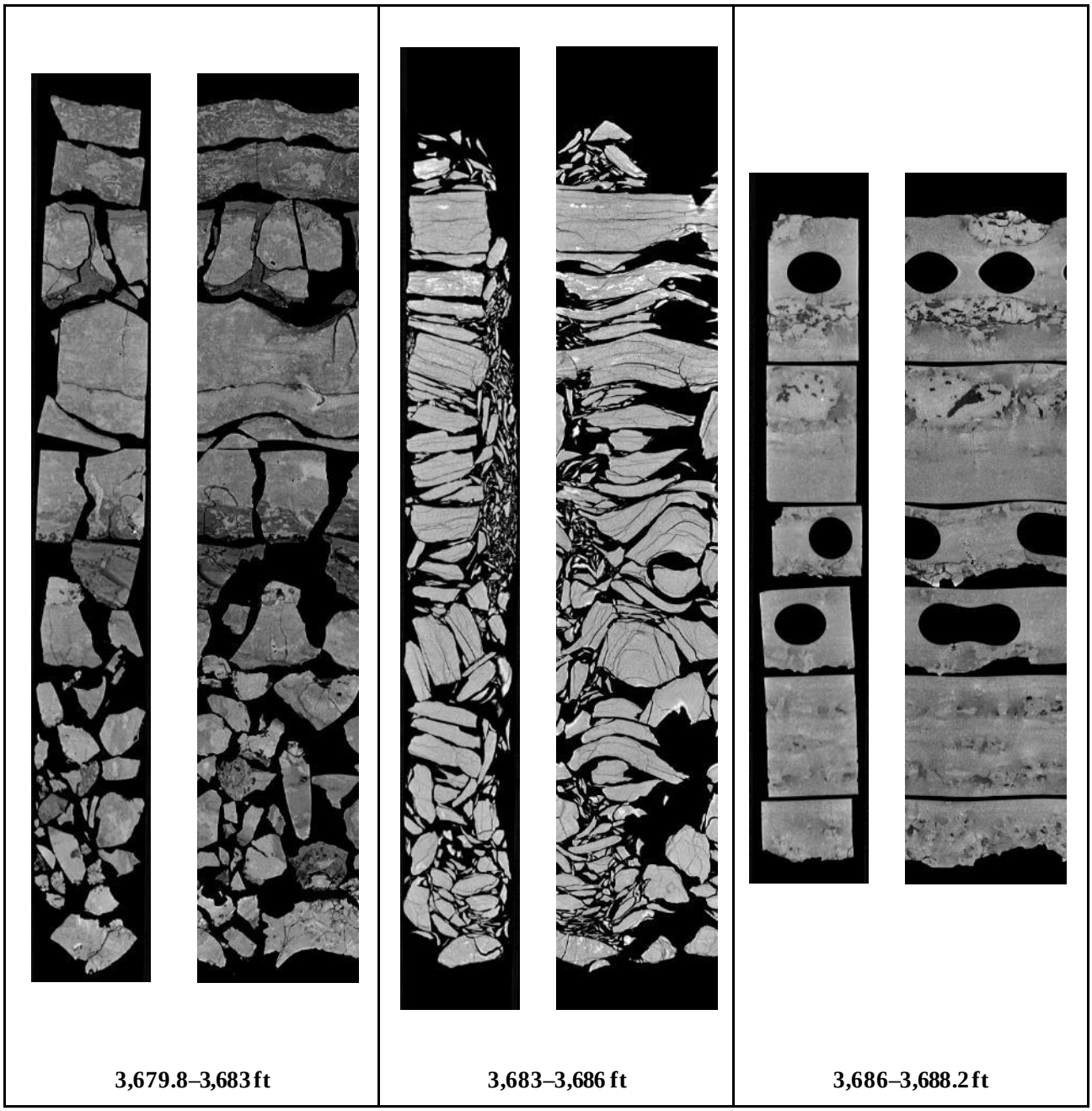

Figure 24: 2D isolated planes through the vertical center and a polar transform of the outside of the medical CT scans of Wellington KGS 2-32 core from 3,679.8–3,688.2 ft.

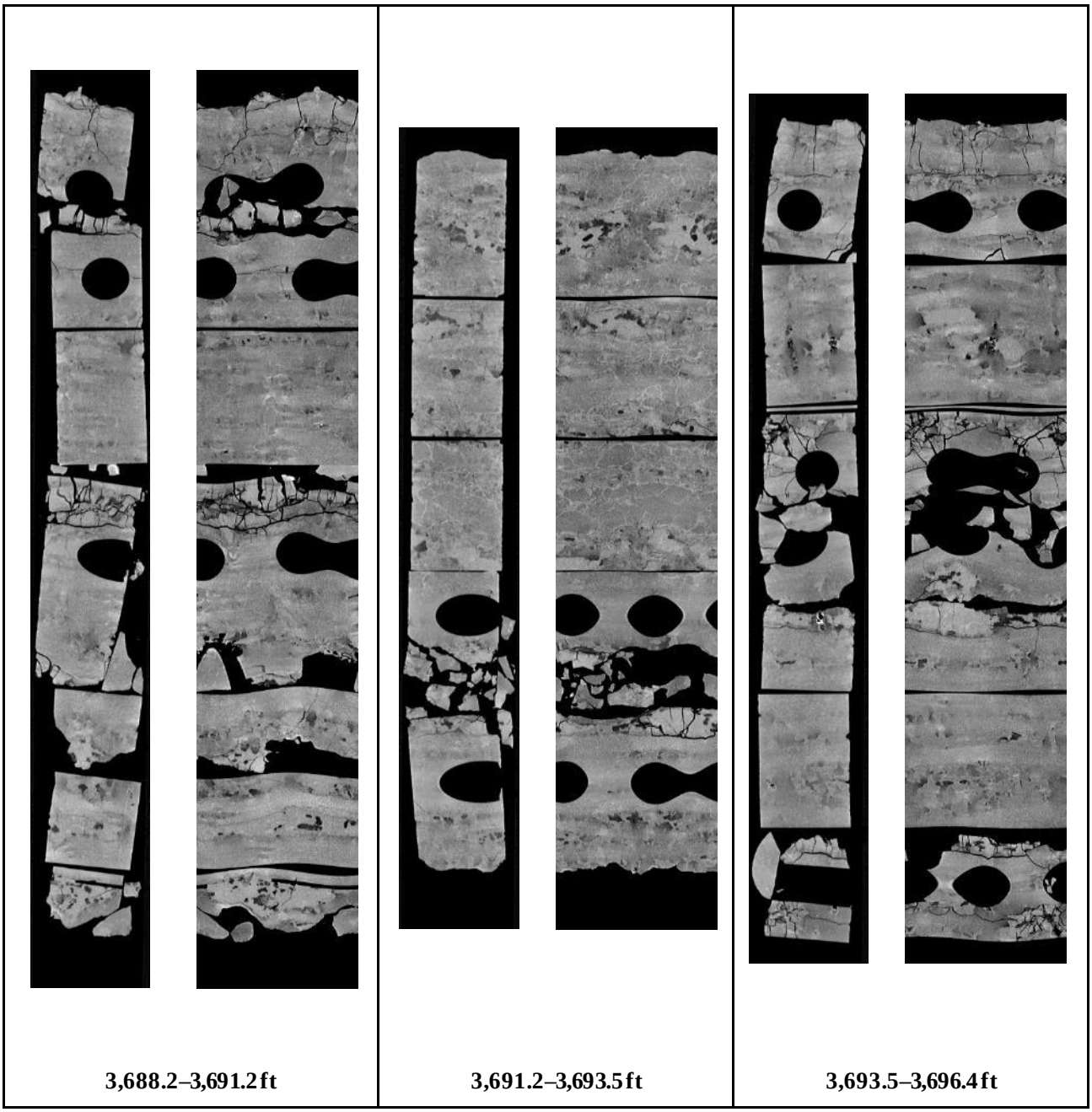

Figure 25: 2D isolated planes through the vertical center and a polar transform of the outside of the medical CT scans of Wellington 2-32 core from 3,688.2–3,696.4 ft.

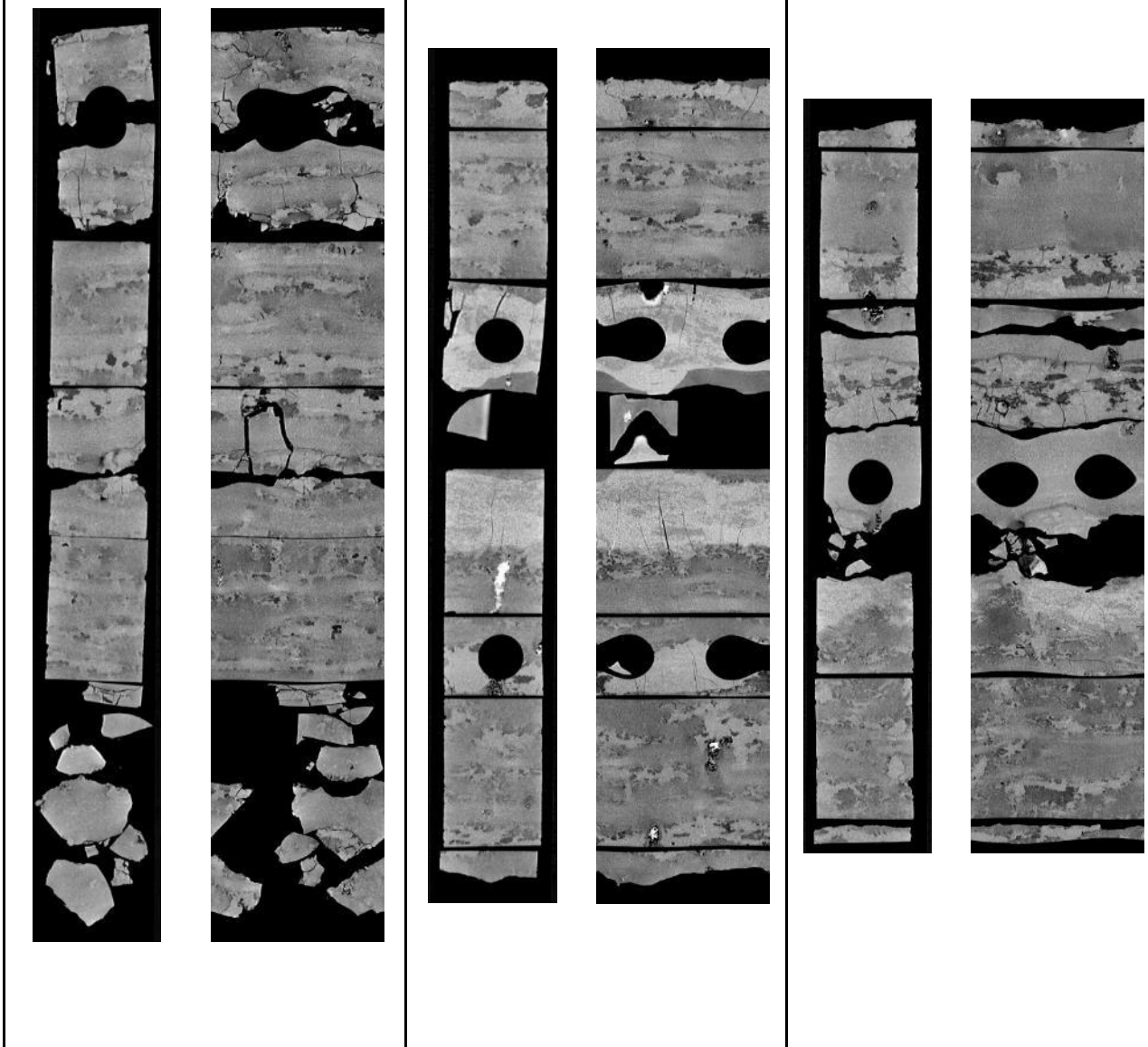

Figure 26: 2D isolated planes through the vertical center and a polar transform of the outside of the medical CT scans of Wellington 2-32 core from 3,696.4–3,703.8 ft.

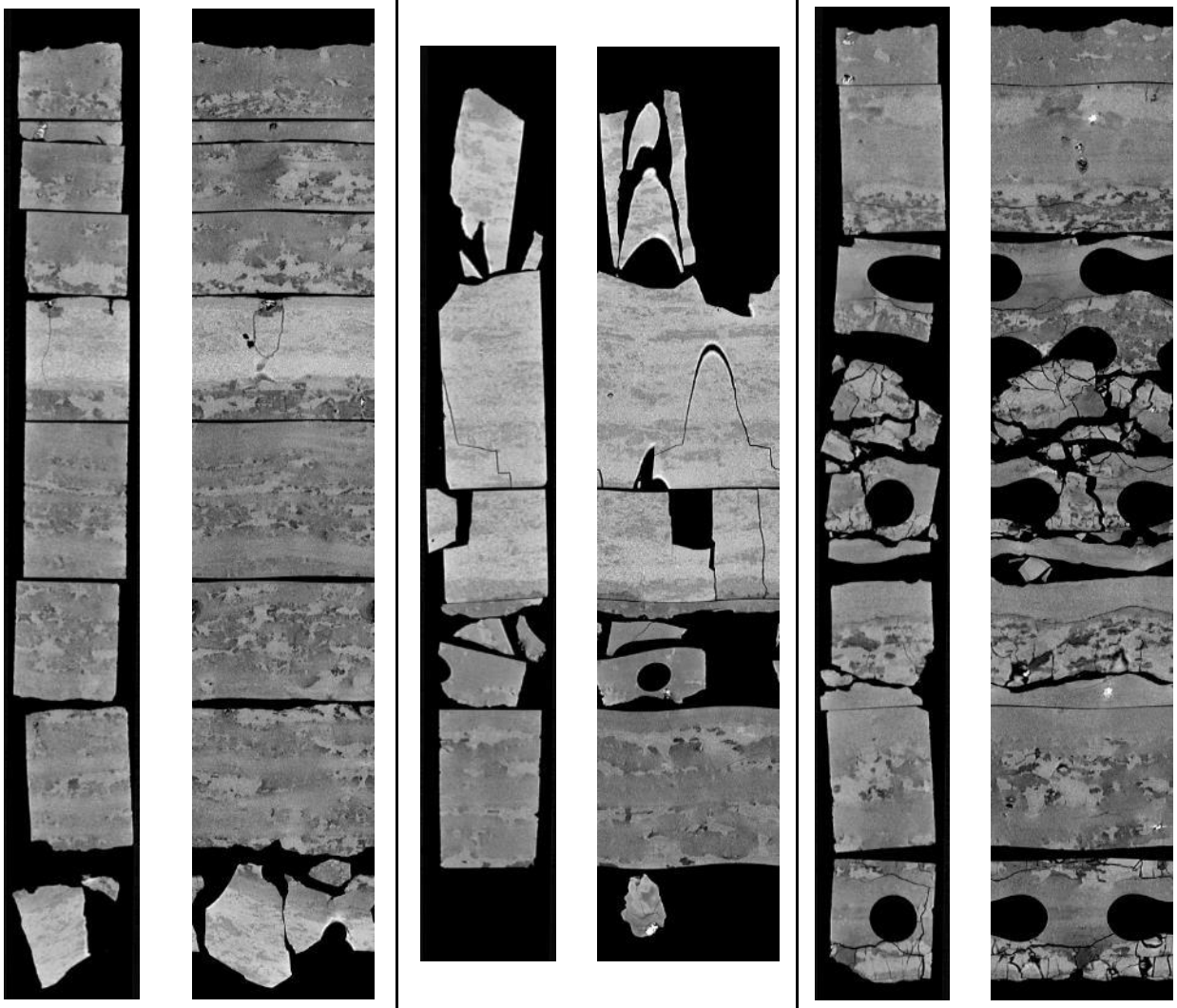

3,703.8–3,707 ft | 3,707–3,708.6 ft | 3,708.6–3,711.9 ft

Figure 27: 2D isolated planes through the vertical center and a polar transform of the outside of the medical CT scans of Wellington KGS 2-32 core from 3,703.8–3,711.9 ft.

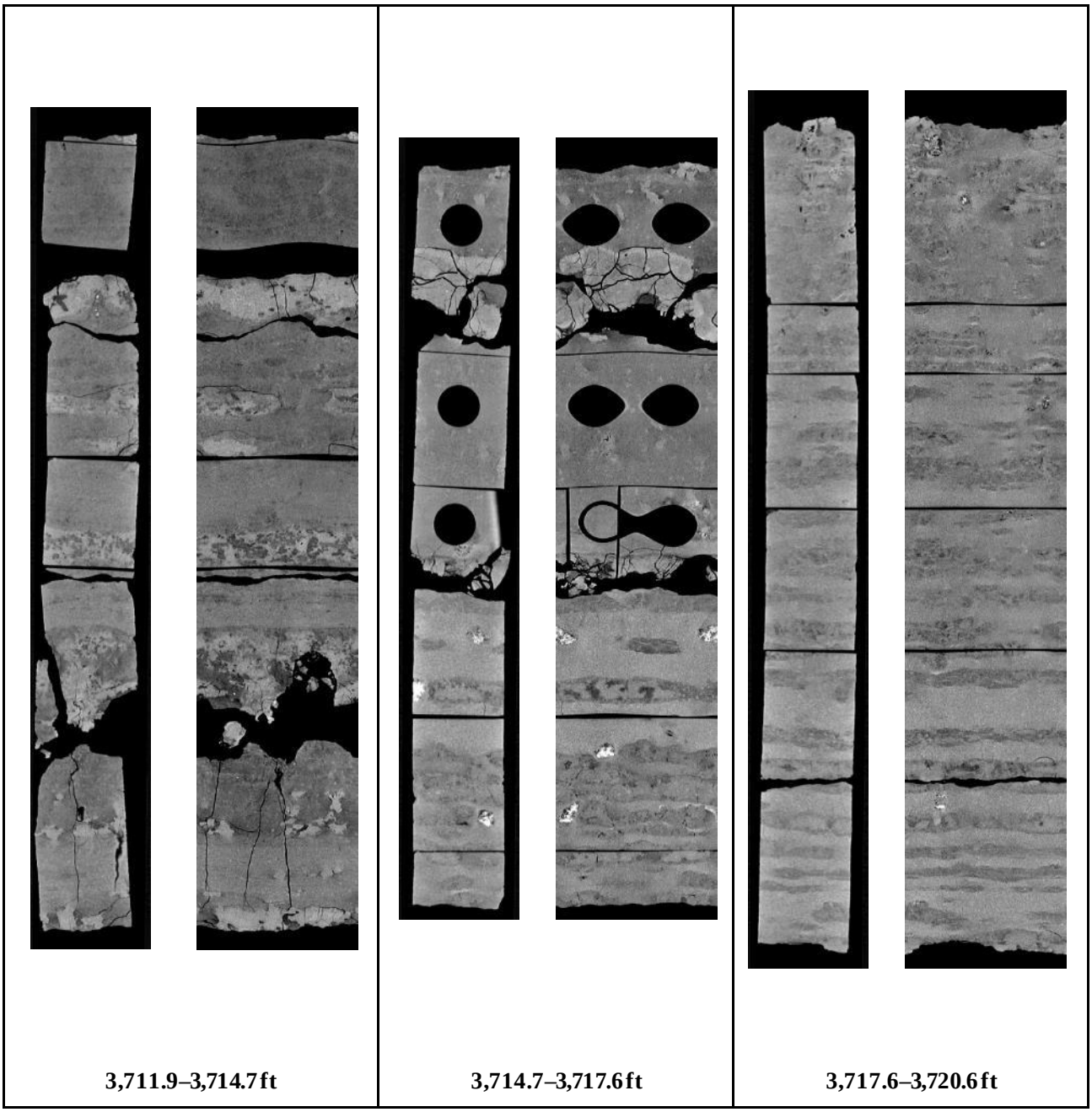

Figure 28: 2D isolated planes through the vertical center and a polar transform of the outside of the medical CT scans of Wellington 2-32 core from 3,711.9–3,720.6 ft.

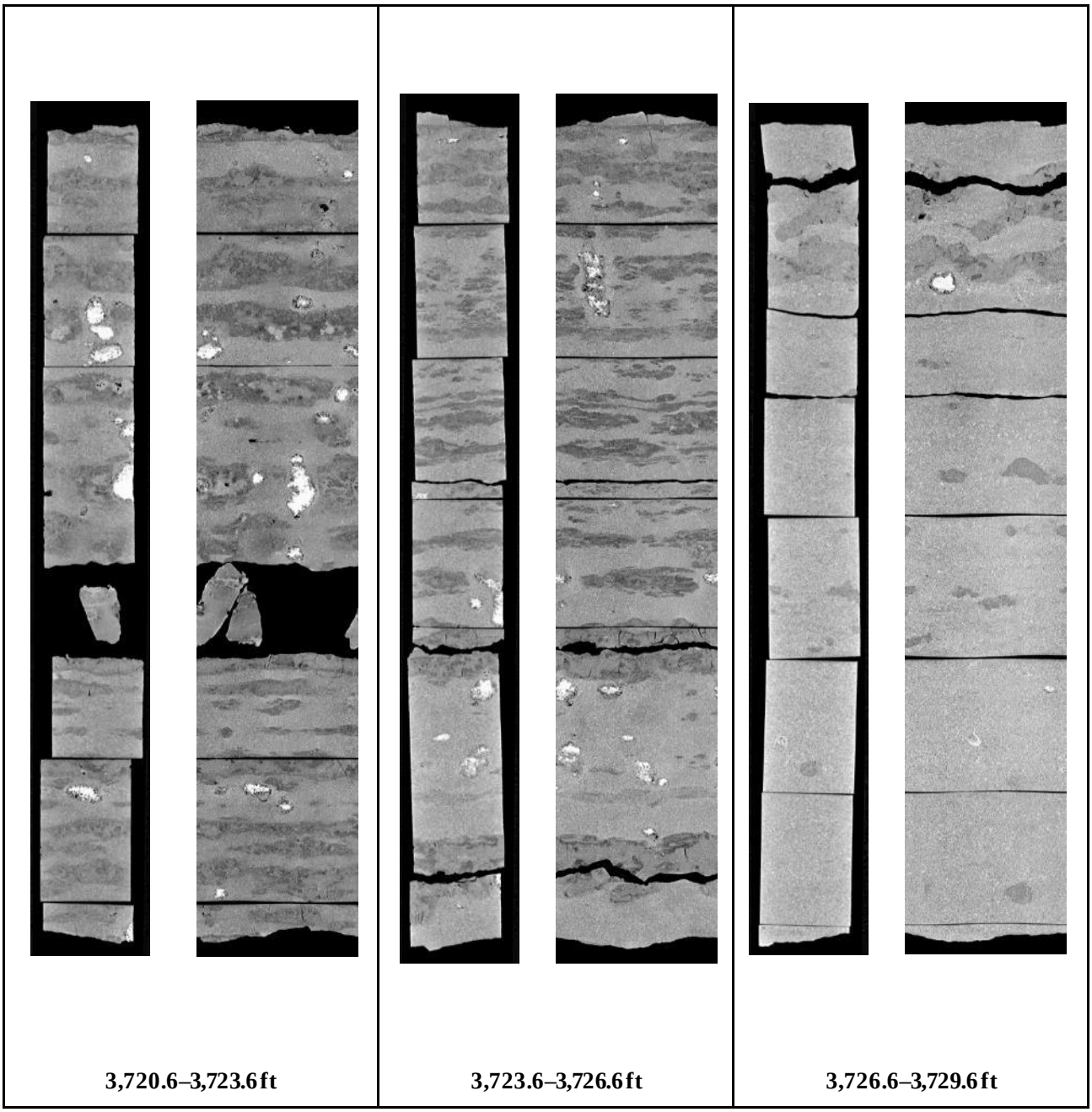

Figure 29: 2D isolated planes through the vertical center and a polar transform of the outside of the medical CT scans of Wellington 2-32 core from 3,720.6–3,729.6 ft.

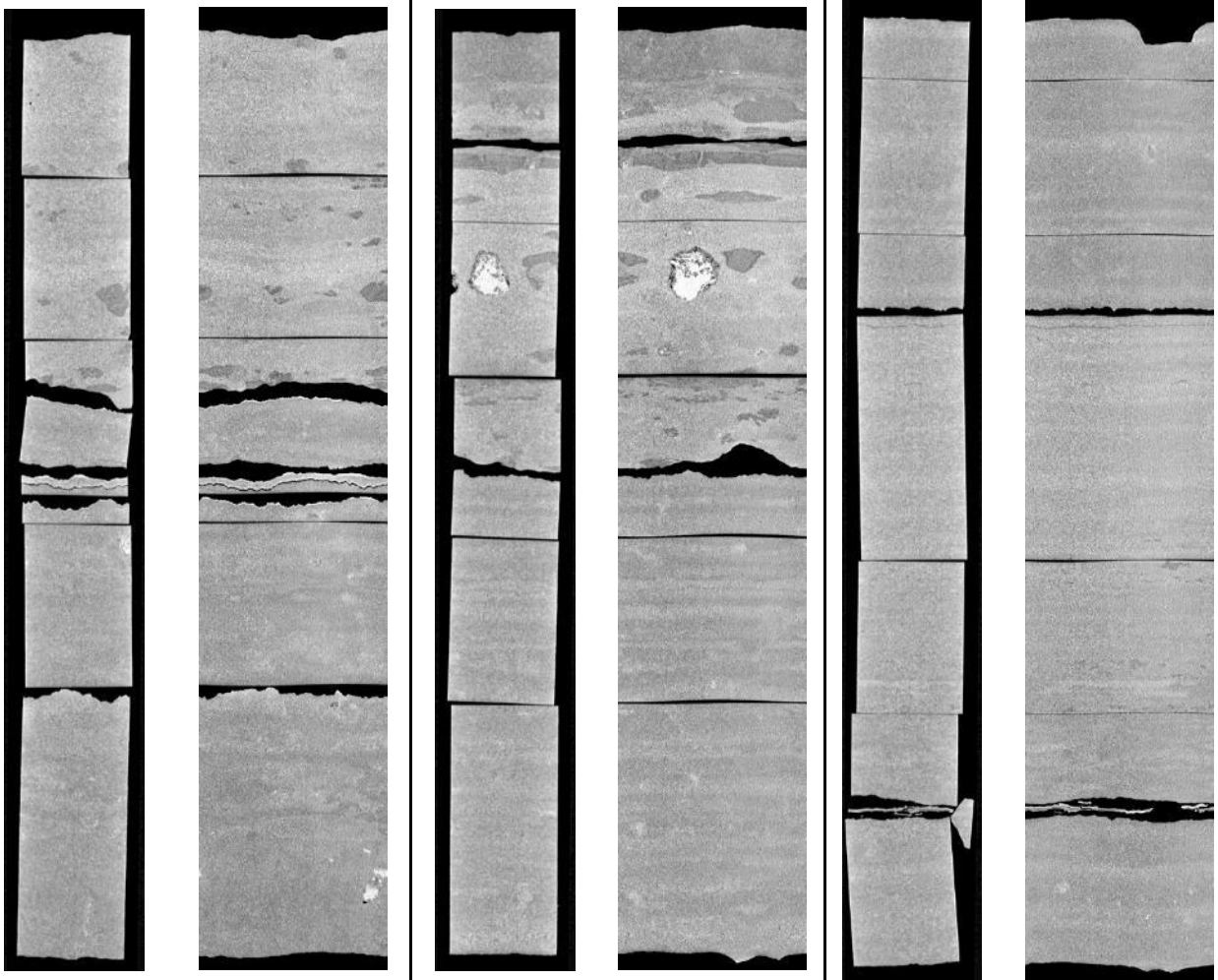

3,729.6–3,732.8 ft | 3,732.8–3,735.3 ft | 3,735.3–3,738.3 ft

Figure 30: 2D isolated planes through the vertical center and a polar transform of the outside of the medical CT scans of Wellington 2-32 core from 3,729.6–3,738.3 ft.

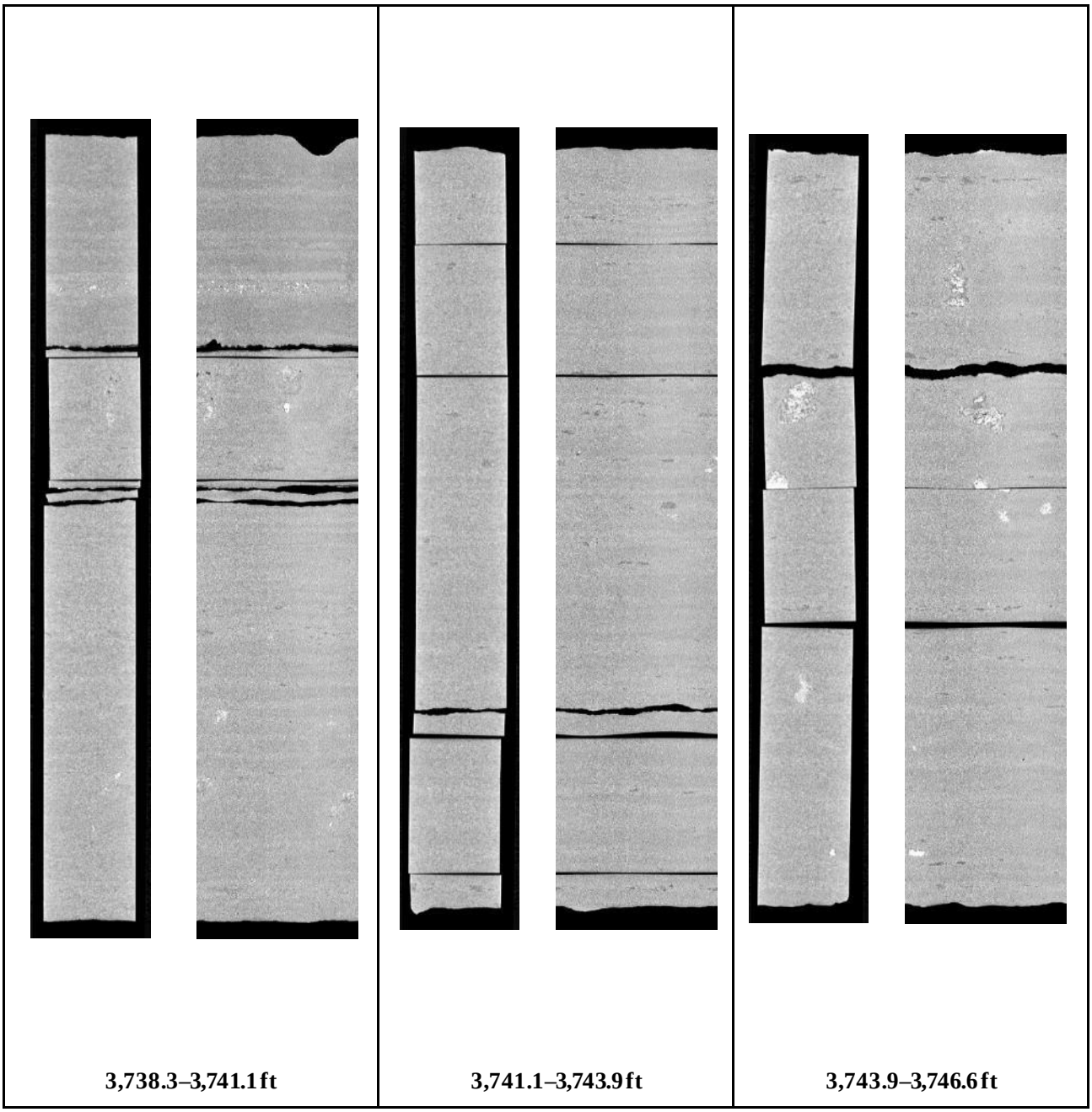

Figure 31: 2D isolated planes through the vertical center and a polar transform of the outside of the medical CT scans of Wellington 2-32 core from 3,738.3–3,746.6 ft.

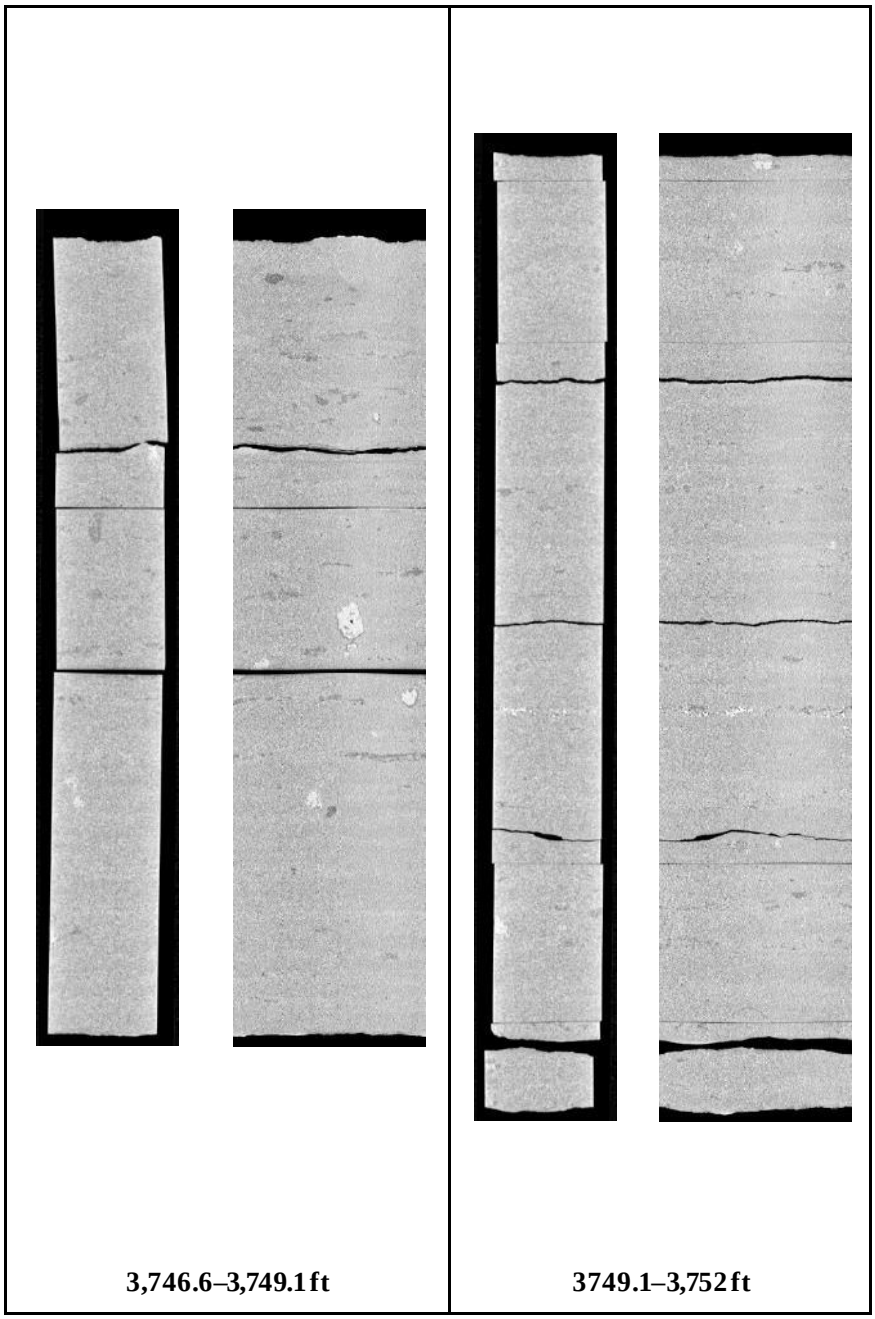

Figure 32: 2D isolated planes through the vertical center and a polar transform of the outside of the medical CT scans of Wellington 2-32 core from 3,746.6–3,752 ft.

3.3 ADDITIONAL CT DATA

Additional CT data can be accessed from NETL's EDX online system using the following link: https://edx.netl.doe.gov/dataset/wellington2-32-core. The original CT data is available as 16-bit tif stacks suitable for reading with ImageJ (Schneider et al., 2012) or other image analysis software.

3.3.1 Medical CT Image Videos

In addition, videos showing the variation along the length of the cross-section images shown in the previous section are available for download and viewing on EDX. A single image from these videos is shown in Figure 33, where the cross section of a mineral filled vug with in a dolomitic and cherty matrix of the core around a depth of 3,702 ft is shown. The red line through the XZ-plane image of the core shows the location of the XY-plane displayed above. The videos on EDX show this XY variation along the entire length of the core.

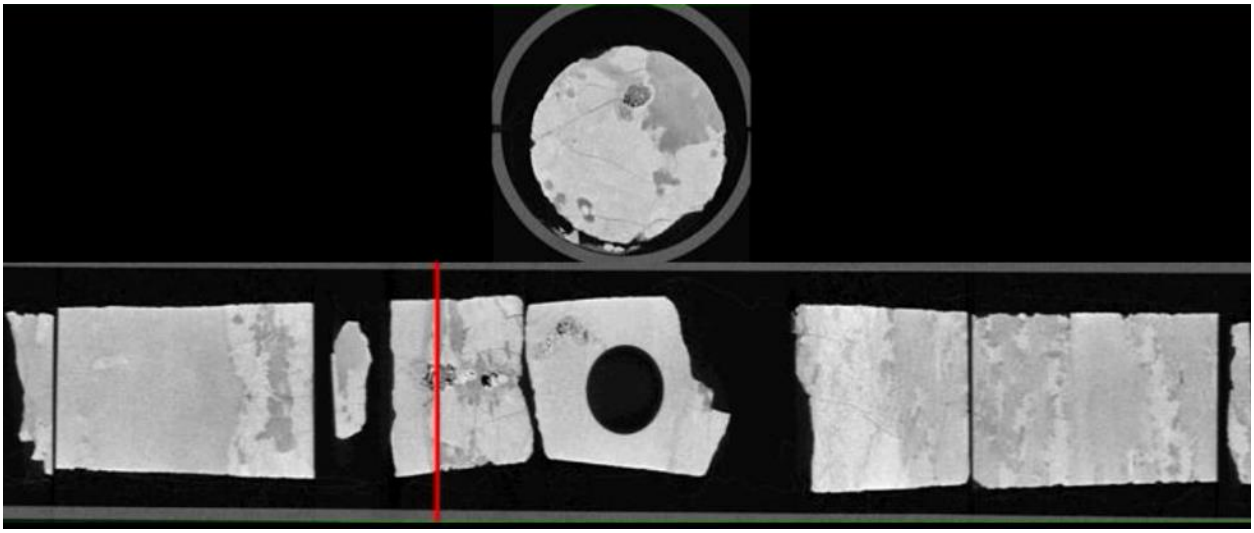

Figure 33: Single image from a video file available on EDX showing variation from 3,701.5–3,703.8 ft. Image above shows the variation in composition within the matrix perpendicular to the core length.

3.3.2 Industrial CT Scans

Detailed industrial CT scans of core sections were performed at NETL. The industrial CT scanner was used to obtain higher resolution images with voxel resolutions between 58 and 67 μm^3 and capture the details of internal features clearly. A listing of the core sections scanned with the industrial CT scanner is shown in Table 2, followed by montages of images through the center of these scans. The "File Name" listed in in Table 2 aligns with the naming sequence of data on EDX, where the full scans are available for download and additional analyses. The montages shown in Figures 34–44 are cross-sections through the center of each core, separated by several mm and illustrate the internal variation in each sample.

Table 2: Industrial Scans of Whole Core

Depth (ft)		File Name	Resolution (µm³)
Top	Bottom		
3,657.22	3,658.59	2-32_CN-1_Bx-2	63.1
3,672.45	3,673.00	2-32_CN-9_Bx-2	63.1
3,674.50	3,675.00	2-32_CN-11_Bx-3	63.1
3,675.48	3,676.00	2-32_CN-12_Bx-3	63.1
3,684.50	3,685.00	2-32_CN-18_Bx-6	63.1
3,694.00	3,694.50	2-32_CN-25_Bx-2	63.1
3,700.15	3,700.65	2-32_CN-64_Bx-4	63.1
3,713.00	3,713.40	2-32_CN-40_Bx-9	67
3,728.00	3,728.50	2-32_CN-49_Bx-14	58
3,741.50	3,742.00	2-32_CN-58_Bx-19	63.1
3,751.30	3,751.80	2-32_CN-63_Bx-22	63.1

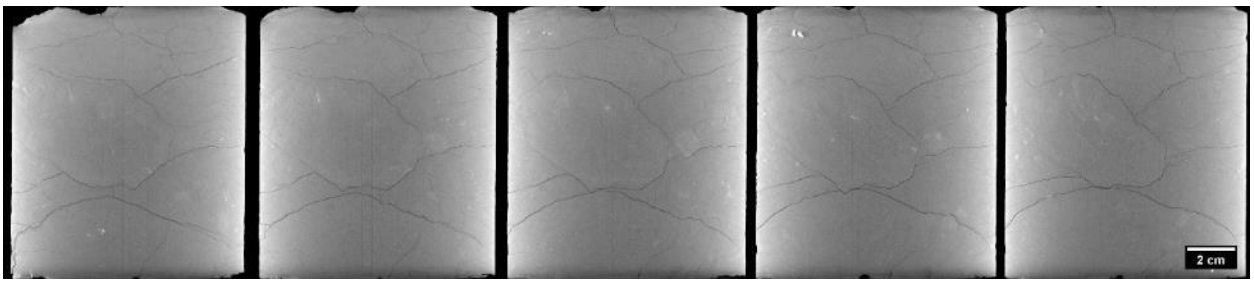

Figure 34: Montage of images through the center of Wellington KGS 2-32 core from 3,657.2–3,658.6 ft scanned with the industrial CT.

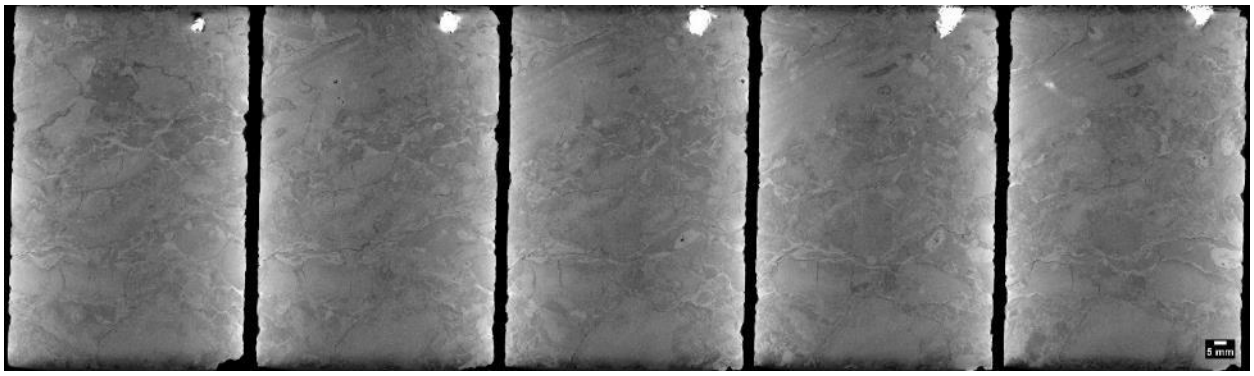

Figure 35: Montage of images through the center of Wellington KGS 2-32 core from 3,672.4–3,673.0 ft scanned with the industrial CT.

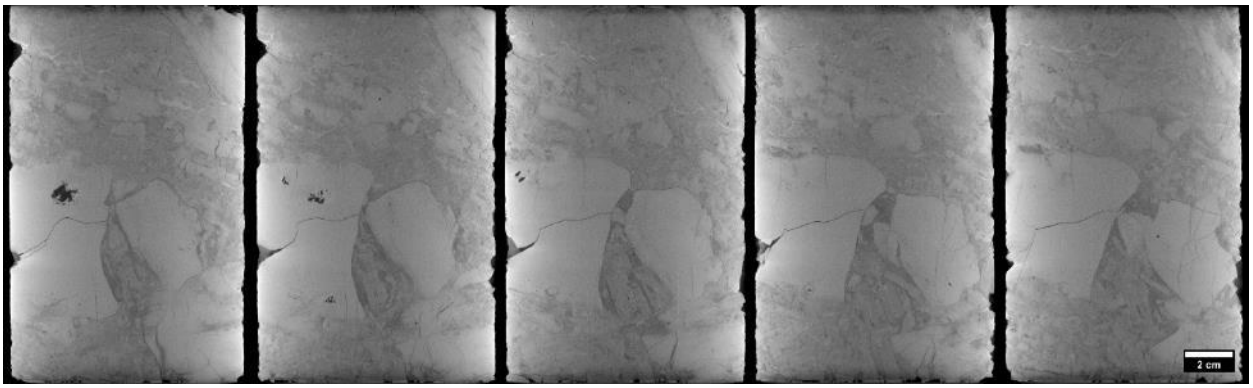

Figure 36: Montage of images through the center of Wellington KGS 2-32 core from 3,674.5–3,675.0 ft scanned with the industrial CT.

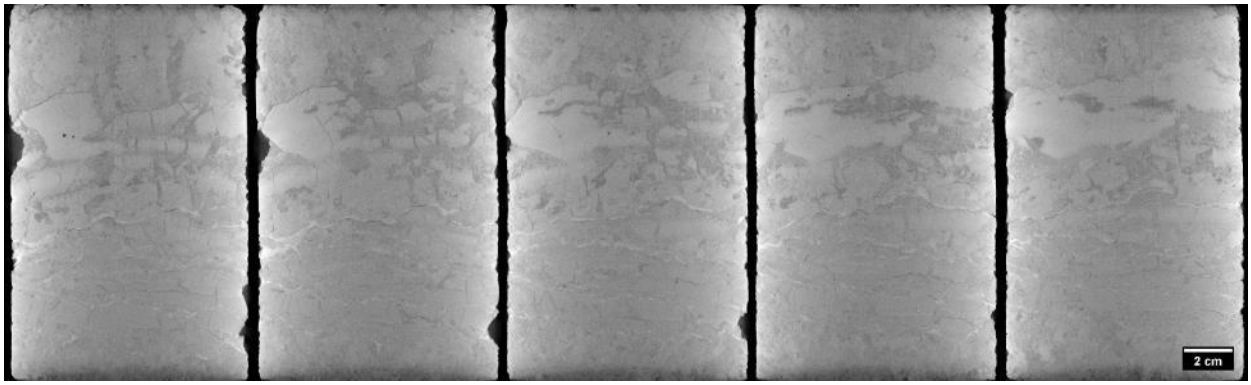

Figure 37: Montage of images through the center of Wellington KGS 2-32 core from 3,675.5–3,676.0 ft scanned with the industrial CT.

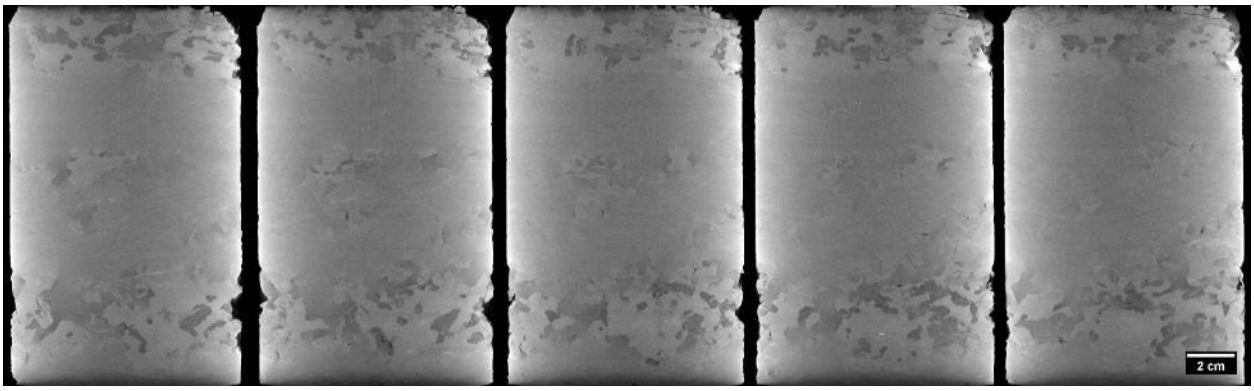

Figure 38: Montage of images through the center of Wellington KGS 2-32 core from 3,684.5–3,685.0 ft scanned with the industrial CT.

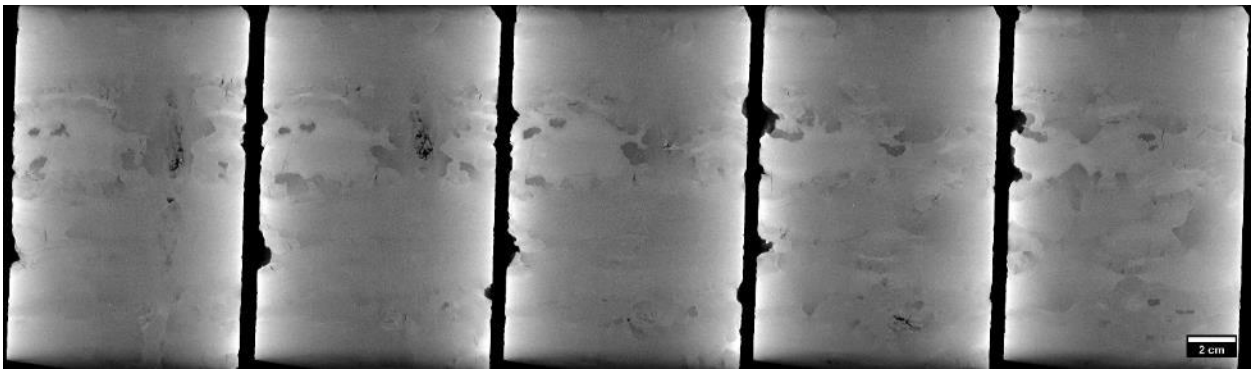

Figure 39: Montage of images through the center of Wellington KGS 2-32 core from 3,694.0–3,694.5 ft scanned with the industrial CT.

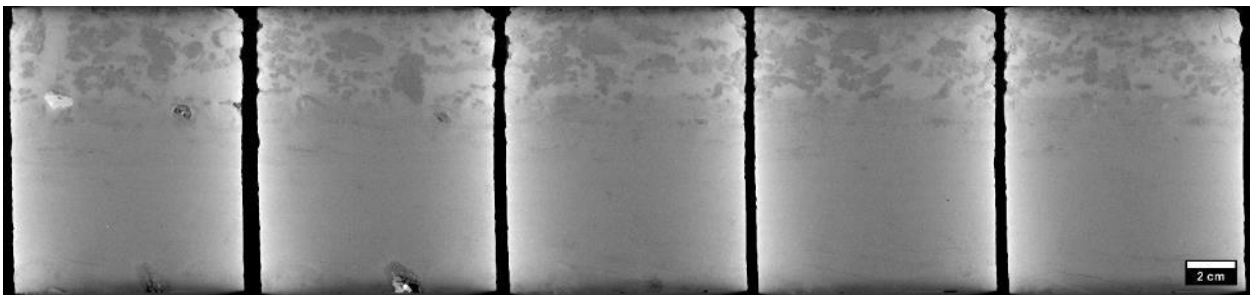

Figure 40: Montage of images through the center of Wellington KGS 2-32 core from 3,713.0–3,713.4 ft scanned with the industrial CT.

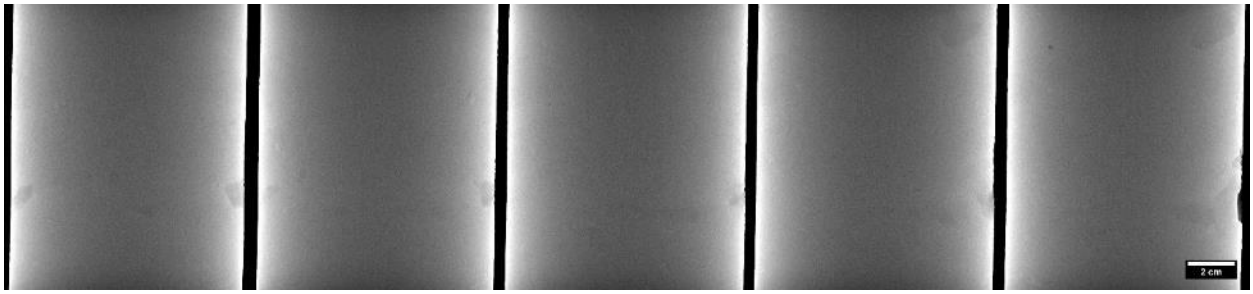

Figure 41: Montage of images through the center of Wellington KGS 2-32 core from 3,728.0–3,728.5 ft scanned with the industrial CT.

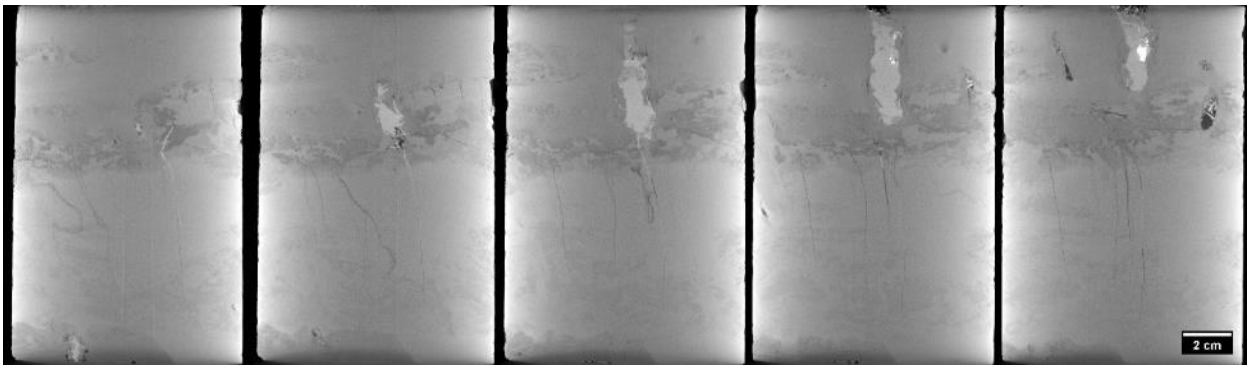

Figure 42: Montage of images through the center of Wellington KGS 2-32 core from 3,700.15–3,700.65 ft scanned with the industrial CT.

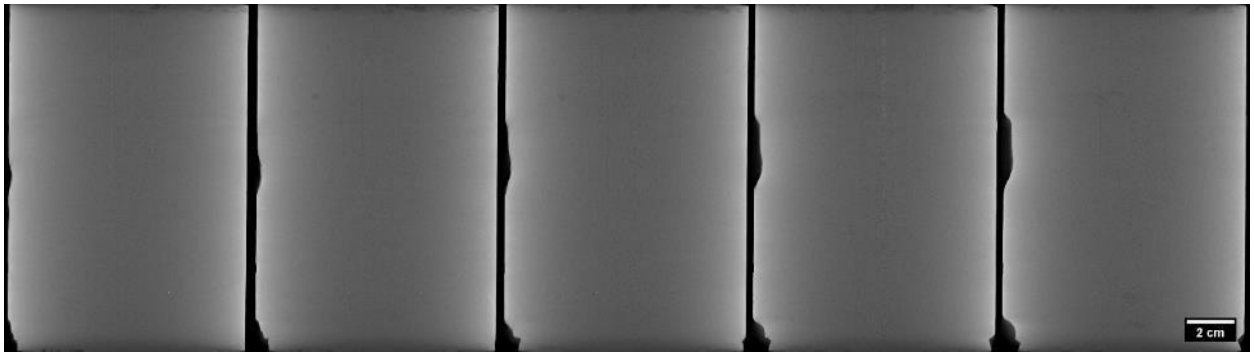

Figure 43: Montage of images through the center of Wellington KGS 2-32 core from 3,741.5–3,742.0 ft scanned with the industrial CT.

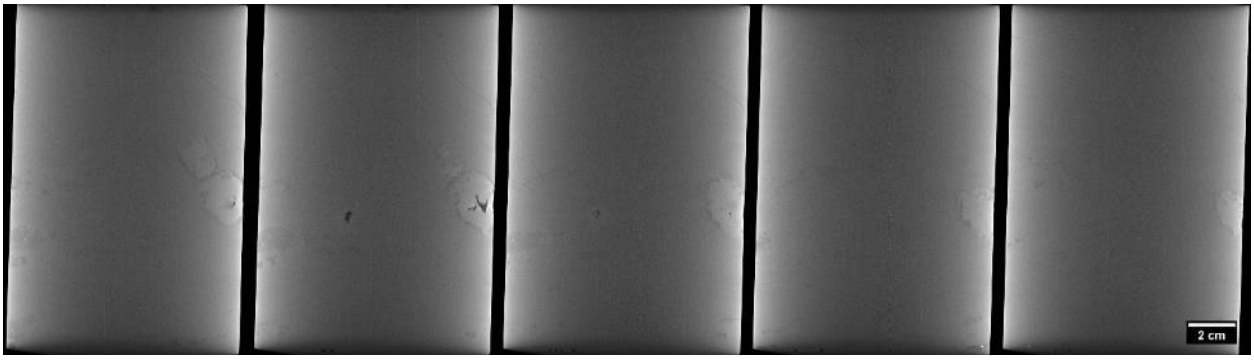

Figure 44: Montage of images through the center of Wellington KGS 2-32 core from 3,751.3–3,751.8 ft scanned with the industrial CT.

3.4 DUAL ENERGY CT SCANNING

Dual energy CT scanning uses two sets of images, produced at different X-ray energies, to approximate the density (ρ_B) (Siddiqui and Khamees, 2004; Johnson, 2012). The technique relies on the use of several standards of known ρ_B to be scanned at the same energies as the specimen. These scans are performed at lower energies (<100 KeV) and higher energies (>100 KeV) to induce two types of photon interactions with the object (Figure 45). The lower energy scans induce photoelectric absorption, which occurs when the energy of the photon is completely absorbed by the object mass and causes ejection of an outer orbital electron (Figure 45a). The high energy scans induce Compton scattering, which causes a secondary emission of a lower energy photon due to incomplete absorption of the photon energy in addition to an electron ejection (Figure 45b).

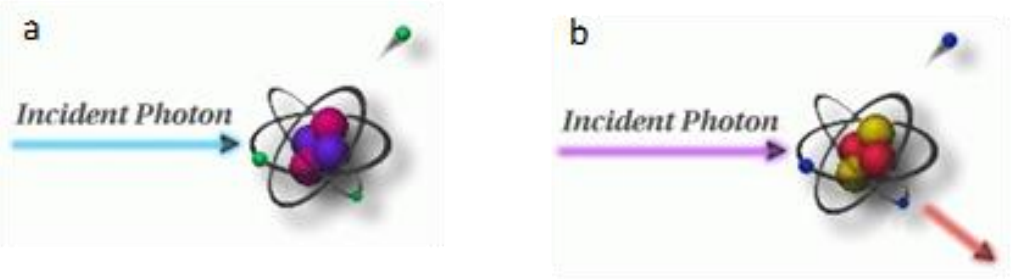

Figure 45: Photon interactions at varying energies: A) Photoelectric absorption, B) Compton scattering. Modified from Iowa State University Center for Nondestructive Evaluation (2021).

Medical grade CT scanners are typically calibrated to known standards, with the output being translated in CTN or Hounsfield Units (HU). Convention for HU defines water as 0 and air as -1,000. A linear transform of recorded HU values is performed to convert them into CTN. This study used CTN as it is the native export format for the medical CT scanner, but it is possible to use HU. Dual energy CT requires at least three calibration points and it is prudent to utilize standards that approximate the object or material of interest. Pure samples of aluminum, graphite, and sodium chloride were used as the calibration standards as they most closely approximate the rocks and minerals of interest (Table 3). Most materials denser than water or with higher atomic masses have a non-linear response to differing CT energies (Table 4).

Table 3: Dual Energy Calibration Standards, Bulk Density (gm/cm^3)

Material	ρ_B (g/cm^3)
Air	-0.001
Water	1
Graphite	2.3
Sodium Chloride	2.16
Aluminum	2.7

Table 4: Dual Energy Calibration Standards, HU and CTN for "Low" and "High" Energies

Material	HU		CTN	
	80 KeV	135 KeV	80 KeV	135 KeV
Air	-993	-994	31,775	31,774
Water	-3.56	-2.09	32,764	32,766
Graphite	381	437	33,149	33,205
Sodium Chloride	1,846	1,237	34,614	34,005
Aluminum	2,683	2,025	35,451	34,793

Dual energy CT utilizes these differences to calibrate to the X-ray spectra. Two equations with three unknowns each are utilized to find ρ_B (Siddiqui and Khamees, 2004):

$$\rho_B = mCTN_{low} + pCTN_{high} + q$$

Where [m, p, and q] and [r, s, and t] are unknown coefficients that can be solved by setting up a system of equations with four 3 x 3 determinants. The CTN is obtained from the CT scans for each of the homogenous calibration standards.

In this study, the high and low energy image stacks were loaded into Python as arrays. A 3D Gaussian blur filter with a sigma of 2 was used to reduce noise in the images. The scipy.solv module of Python was then employed to solve for the coefficients based on the calibration CTN values. The ρ_B was solved for each pixel in the 3D volume and saved as two new separate image stacks.

3.5 COMPILED CORE LOG

The compiled core logs were scaled to fit on single pages for rapid review of the combined data from the medical CT scans and MSCL readings. Two sets of logs are presented for the core: the first set with data from the CT scans and XRF, and the second set with calculated ratios from the XRF scans, P-wave data, and notable features. Features that can be derived from these combined analyses include determination of mineral locations, such as pyrite, from magnetic susceptibility and using the XRF to inform geochemical composition and mineral form.

Data from the MSCL with P-wave velocity less than 330 m/s has been removed from these logs. This low P-wave velocity is less than the anticipated velocity through air, indicating a highly fractured zone and unreliable readings. The location of these fractured zones was confirmed through visual examination and with the medical CT scanned images.

The elemental results from the XRF were limited to light elements, Ca, and Si, and the remaining top nine elements (Al, Mg, Ti, S, Fe, Mn, Cl, Zn, and V). Of the remaining top nine elements, Mg was the most abundant with a maximum occurrence of 101,331 ppm at one location in the core, followed by Al with a maximum occurrence of 97,456 ppm. Zn had the lowest maximum occurrence with 526.41 ppm, all other elements had maximum occurrences less than 500 ppm.

Trends in elemental ratios can provide insight into mineral composition. Examples include:

- Ca/Si, provides information of carbonate to chert/detrital influence
- Si/Al, provides information on the abundance of illite and micas versus other clays, and the abundance of cherts to clays
- Mn/Fe and S/Fe, can provide information in redox trends
- Mg/Ca, provides information on the abundance of dolomite to calcite (note there is no information in the top portion of the well due to the presence of siliciclastic rocks)
- Magnetic susceptibility can test for iron sulfides (reducing) or oxidized Fe and sulfate. Pyrite (reduced) should have low magnetic susceptibility. Additionally, magnetic susceptibility in "normal" rock matrices (carbonate and siliciclastic) have low magnetic susceptibility values.
- Fe oxide or hydroxide, should have high magnetic susceptibility

These broad trends can quickly give information on large suites of core and direct more focused research (Figure 46 and Figure 47).

Additionally, a plate representing Wellington KGS 2-32 is available on EDX (https://edx.netl.doe.gov/dataset/wellington2-32-core). This plate shows all the data compiled in this report (except the industrial CT scans) in a raster log and provides a more detailed visual representation of the well. The header provides the general log information and where the data in the log plots is sourced. This plot (Figure 48) contains:

- The lithology description
- Density from the MSCL gamma density, dual energy density, and log density
- Magnetic susceptibility (MS1)
- P-wave Velocity (PWVel)
- Dual energy density CT-image reslices with royal LUT
- Polar transform CT-image slices
- KGS core data (whole core permeability (max and vertical))
- Whole core porosity, and water and oil saturations
- XRF mineralogy (quartz (Si), clay (Al), calcite (Ca), and dolomite (Mg))
- Lithology proxies (Si, Ca, Al, K, Mg, Zr, Mn, Fe, and S)
- Redox proxies (Mo, V, Cr, Cu)
- Paleoproductivity proxies (P, Zn, Ni, and Pb)

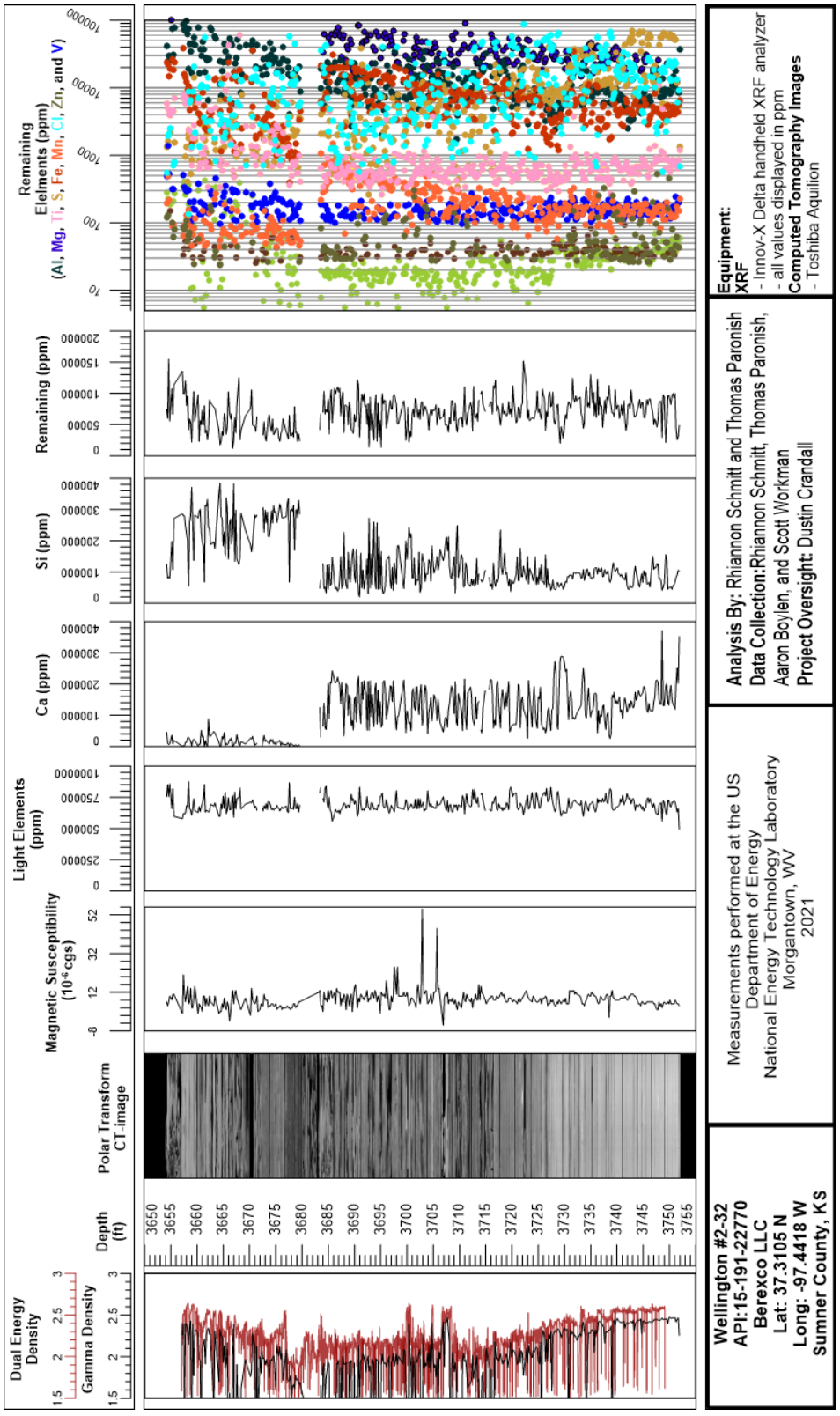

Figure 46: Compiled core log for Wellington #2-32 Well, from 3,654–3,752 ft.

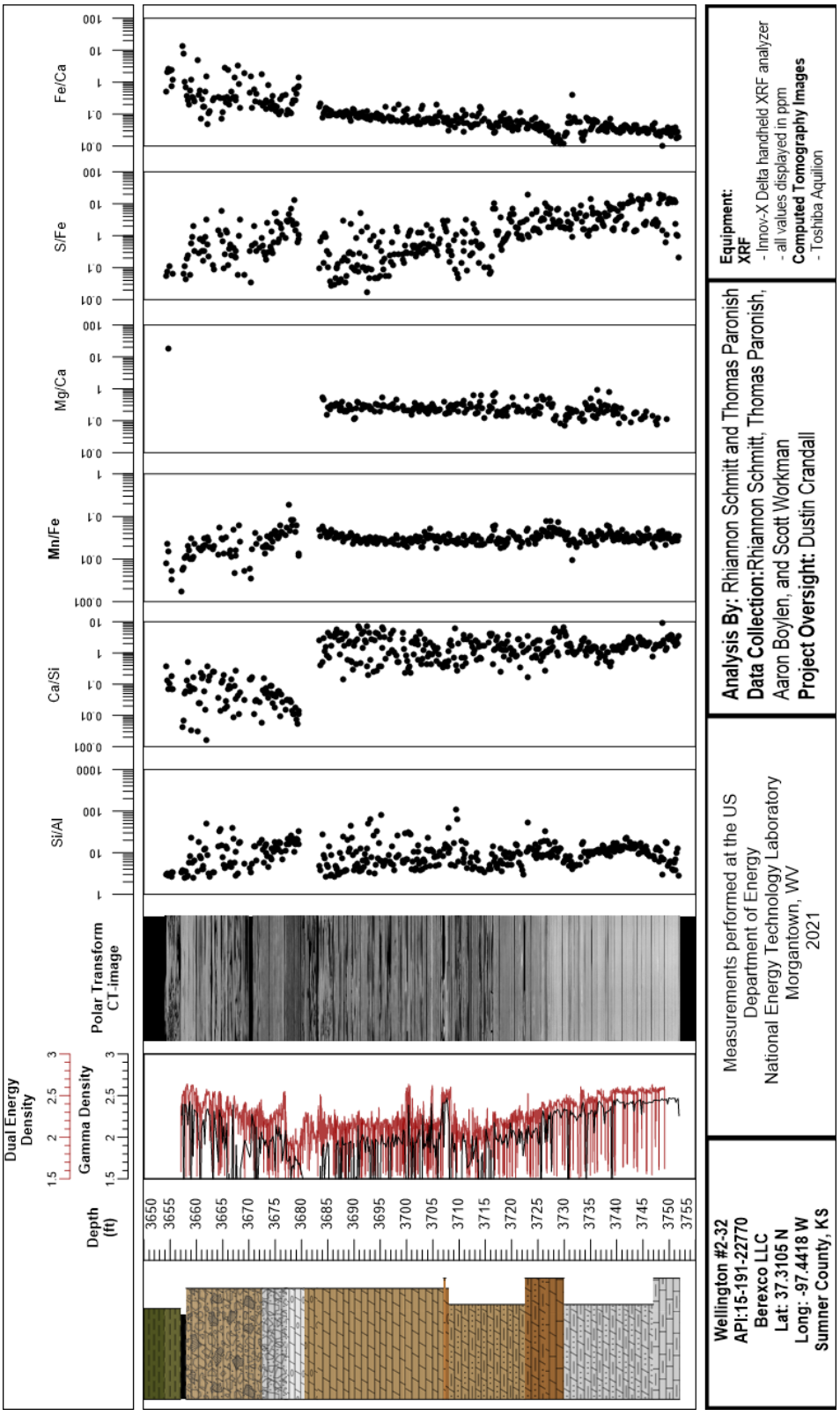

Figure 47: Compiled core log with elemental ratios for Wellington #2-32 Well, from 3,654–3,752 ft.

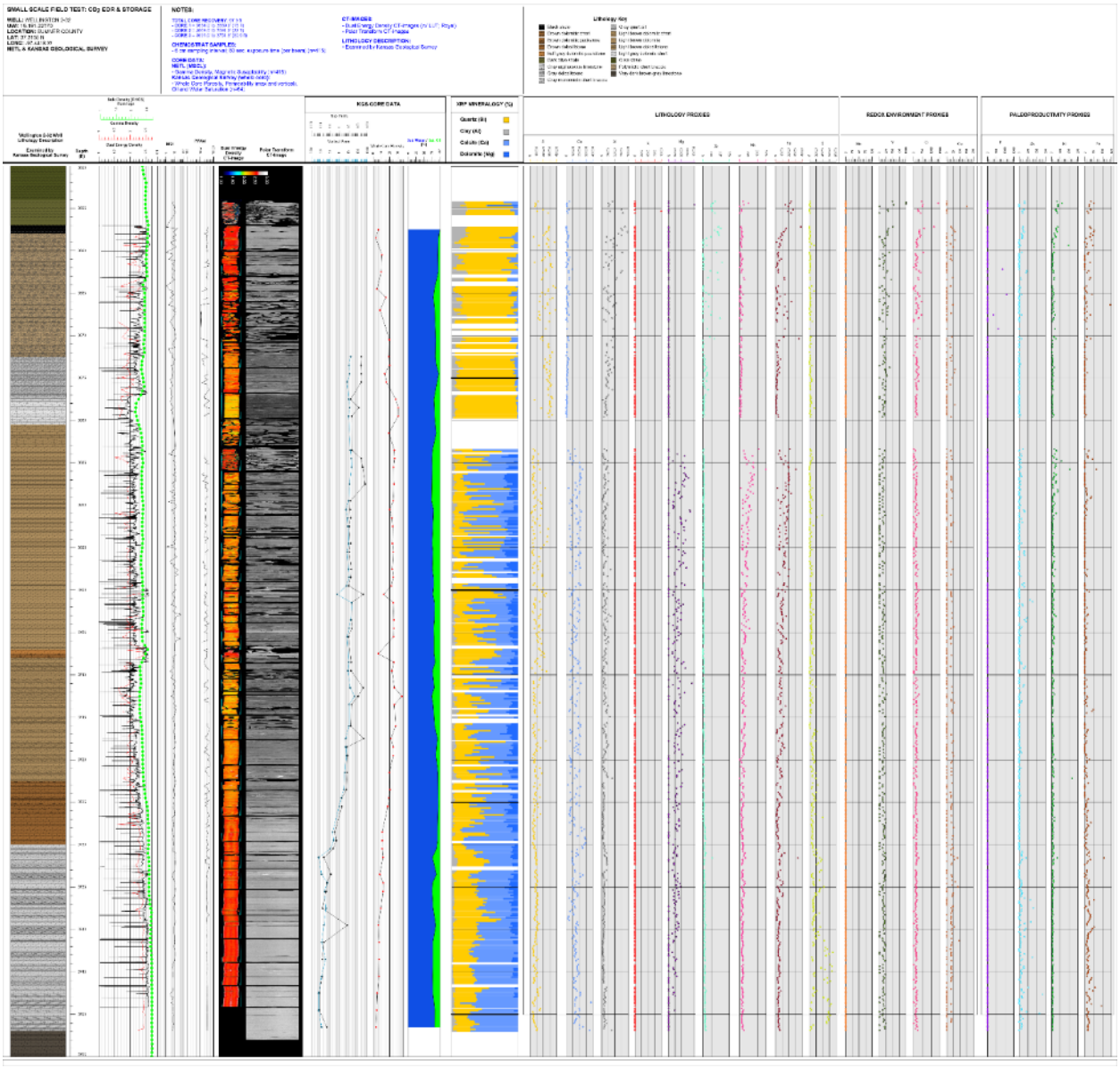

Figure 48: Combined core characterization for the Wellington KGS 2-32 well. For the full-size version visit EDX (https://edx.netl.doe.gov/dataset/wellington2-32-core).

4. DISCUSSION

The measurements of the magnetic susceptibility, P-wave velocity, XRF, and CT analysis provide a unique look into of the internal structure of the core and macroscopic changes in lithology. These techniques:

- Are non-destructive
- When performed in parallel, give insight into the core beyond what one individual technique can provide
- Can be used to identify zones of interest for detailed analysis, experimentation, and quantification
- Provide a detailed digital record of the core, before any destructive testing or further degradation, that is accessible and can be referenced for future studies

5. REFERENCES

Evans, C. S.; Newell, K. D. *The Mississippian Limestone Play in Kansas: Oil and gas in a complex geologic setting*; Kansas Geological Survey, Geology Extension, University of Kansas, 2013.

Geotek Ltd. Multi-Sensor Core Logger Manual; Version 05-10; Published by Geotek, 3 Faraday Close, Daventry, Northamptonshire NN11 8RD, 2010. info@geotek.co.uk, www.geotek.co.uk

Holubnyak, Y. E.; Watney, L.; Hollenbach, J.; Birdie, T.; Fazelalavi, M.; Bidgoli, T.; Schwab, D.; Nolte, A.; Tsoflias, G.; Victorine, J.; Graham, B.; Doveton, J.; Bruns, J.; Blazer, B; Wreath, D. *Small Scale Field Test Demonstrating CO_2 Sequestration in Arbuckle Saline Aquifer and by CO_2-Enhanced Oil Recovery at Wellington Field, Sumner County, Kansas;* Final Report for DE-FE0006821; 2017. https://www.netl.doe.gov/sites/default/files/2018-02/DE-FE00006821-Final-reportV6.pdf (accessed 2021).

Hunts, C.; Moskowitz, B.; Banerjee, S. Magnetic Properties of Rocks and Minerals*;* In *Rock Physics and Phase Relations: A Handbook of Physical Constants*; 1995; pp 189–204.

Iowa State University Center for Nondestructive Evaluation, Ames, IA, 2021. https://www.nde-ed.org/Physics/X-Ray/attenuation.xhtml (accessed July 2021).

Johnson, T. R. C. Dual-Energy CT: General Principles. *American Journal of Roentgenology* **2012,** *199*, S3–S8. DOI: 10.2214/AJR.12.9116.

KGS. Kansas Geological Survey. Digital Petroleum Atlas. Structure with Oil production, Mississippian; 1998. https://www.kgs.ku.edu/DPA/Plays/ProdMaps/miss_oil.html (accessed 2021).

KGS. Kansas Geological Survey. Kansas Oil and Gas Well Database, Specific Well—15-191-22770; 2015. https://chasm.kgs.ku.edu/ords/qualified.well_page.DisplayWell?f_kid=1044998939 (accessed 2021).

KGS. Kansas Geological Survey. KGS Website, 2021. https://www.kgs.ku.edu/ (accessed 2021).

Scheffer, A. Geochemical and Microbiological Characterization of the Arbuckle Saline Aquifer, a Potential CO_2 Storage Reservoir; Implications for Hydraulic Separation and Caprock Integrity. MS Thesis, Kansas University, 2012. https://kuscholarworks.ku.edu/handle/1808/13016

Schneider, C. A.; Rasband, W. S.; Eliceiri, K. W. NIH Image to ImageJ: 25 years of image analysis. *Nature Methods* **2012,** *9*, 671–675.

Siddiqui, S.; Khamees, A. A. Dual-Energy CT-Scanning Applications in Rock Characterization. *Society of Petroleum Engineers* **2004**. DOI:10.2118/90520-MS.

Watney, W. L.; Guy, W. J.; Byrnes, A. P. *Characterization of the Mississippian Osage chat in south-central Kansas*; Open-file Report 2002-50; Kansas Geological Survey, 2002. http://www.kgs.ku.edu/PRS/Poster/2002/2002-50/index.html (accessed 2021).

Watney, W. L.; Holubnyak, Y. E.; Birdie, T.; Hollenbach, J. Small Scale Field Test Demonstrating CO_2 Sequestration in Arbuckle Saline Aquifer and by CO_2-Enhanced Oil Recovery at Wellington Field, Sumner County, Kansas DE-FE0006821. Mastering the Subsurface through Technology Innovation, Partnerships and Collaboration: Carbon Storage and Oil and Natural Gas Technologies Review Meeting: Pittsburgh, PA, Aug 3, 2017. https://www.netl.doe.gov/sites/default/files/2017-11/Yevhen--Eugene--Holubnyak-DE-FE0006821-2017-Small-Scale-Annual-review-meeting.pdf (accessed 2021)

Brian Anderson
Director
National Energy Technology Laboratory
U.S. Department of Energy

Darin Damiani
Carbon Storage Program Manager
Office of Carbon Management
U.S. Department of Energy

Mark McKoy
Carbon Storage Technology Director
National Energy Technology Laboratory
U.S. Department of Energy

Bryan Morreale
Executive Director
Research and Innovation Center
National Energy Technology Laboratory
U.S. Department of Energy

NETL Technical Report Series